

Absolute Measurements of Branching Fractions of Cabibbo-Suppressed Hadronic $D^{0(+)}$ Decays Involving Multiple Pions

M. Ablikim¹, M. N. Achasov^{11,b}, P. Adlarson⁷¹, M. Albrecht⁴, R. Aliberti³¹, A. Amoroso^{70A,70C}, M. R. An³⁵, Q. An^{67,53}, X. H. Bai⁶¹, Y. Bai⁵², O. Bakina³², R. Baldini Ferroli^{26A}, I. Balossino^{27A}, Y. Ban^{42,g}, V. Batzskaya^{1,40}, D. Becker³¹, K. Begzsuren²⁹, N. Berger³¹, M. Bertani^{26A}, D. Bettoni^{27A}, F. Bianchi^{70A,70C}, J. Bloms⁶⁴, A. Bortone^{70A,70C}, I. Boyko³², R. A. Briere⁵, A. Brueggemann⁶⁴, H. Cai⁷², X. Cai^{1,53}, A. Calcaterra^{26A}, G. F. Cao^{1,58}, N. Cao^{1,58}, S. A. Cetin^{57A}, J. F. Chang^{1,53}, W. L. Chang^{1,58}, G. Chelkov^{32,a}, C. Chen³⁹, G. Chen¹, H. S. Chen^{1,58}, M. L. Chen^{1,53}, S. J. Chen³⁸, T. Chen¹, X. R. Chen^{28,58}, X. T. Chen¹, Y. B. Chen^{1,53}, Z. J. Chen^{23,h}, W. S. Cheng^{70C}, X. Chu³⁹, G. Cibinetto^{27A}, F. Cossio^{70C}, J. J. Cui⁴⁵, H. L. Dai^{1,53}, J. P. Dai⁷⁴, A. Dbeyssi¹⁷, R. E. de Boer⁴, D. Dedovich³², Z. Y. Deng¹, A. Denig³¹, I. Denysenko³², M. Destefanis^{70A,70C}, F. De Mori^{70A,70C}, Y. Ding³⁶, J. Dong^{1,53}, L. Y. Dong^{1,58}, M. Y. Dong^{1,53,58}, X. Dong⁷², S. X. Du⁷⁶, P. Egorov^{32,a}, Y. L. Fan⁷², J. Fang^{1,53}, S. S. Fang^{1,58}, W. X. Fang¹, Y. Fang¹, R. Farinelli^{27A}, L. Fava^{70B,70C}, F. Feldbauer⁴, G. Felici^{26A}, C. Q. Feng^{67,53}, J. H. Feng⁵⁴, K. Fischer⁶⁵, M. Fritsch⁴, C. Fritsch⁶⁴, C. D. Fu¹, H. Gao⁵⁸, Y. N. Gao^{42,g}, Yang Gao^{67,53}, S. Garbolino^{70C}, I. Garzia^{27A,27B}, P. T. Ge⁷², Z. W. Ge³⁸, C. Geng⁵⁴, E. M. Gersabeck⁶², A. Gilman⁶⁵, K. Goetzen¹², L. Gong³⁶, W. X. Gong^{1,53}, W. Gradl³¹, M. Greco^{70A,70C}, L. M. Gu³⁸, M. H. Gu^{1,53}, Y. T. Gu¹⁴, C. Y. Guan^{1,58}, A. Q. Guo^{28,58}, L. B. Guo³⁷, R. P. Guo⁴⁴, Y. P. Guo^{10,f}, A. Guskov^{32,a}, T. T. Han⁴⁵, W. Y. Han³⁵, X. Q. Hao¹⁸, F. A. Harris⁶⁰, K. K. He⁵⁰, K. L. He^{1,58}, F. H. Heinsius⁴, C. H. Heinz³¹, Y. K. Heng^{1,53,58}, C. Herold⁵⁵, M. Himmelreich^{12,d}, T. Holtmann⁴, G. Y. Hou^{1,58}, Y. R. Hou⁵⁸, Z. L. Hou¹, H. M. Hu^{1,58}, J. F. Hu^{51,i}, T. Hu^{1,53,58}, Y. Hu¹, G. S. Huang^{67,53}, K. X. Huang⁵⁴, L. Q. Huang^{28,58}, L. Q. Huang⁶⁸, X. T. Huang⁴⁵, Y. P. Huang¹, Z. Huang^{42,g}, T. Hussain⁶⁹, N. Hüsken^{25,31}, W. Imoehl²⁵, M. Irshad^{67,53}, J. Jackson²⁵, S. Jaeger⁴, S. Janchiv²⁹, Q. Ji¹, Q. P. Ji¹⁸, X. B. Ji^{1,58}, X. L. Ji^{1,53}, Y. Y. Ji⁴⁵, Z. K. Jia^{67,53}, H. B. Jiang⁴⁵, S. S. Jiang³⁵, X. S. Jiang^{1,53,58}, Y. Jiang⁵⁸, J. B. Jiao⁴⁵, Z. Jiao²¹, S. Jin³⁸, Y. Jin⁶¹, M. Q. Jing^{1,58}, T. Johansson⁷¹, N. Kalantar-Nayestanaki⁵⁹, X. S. Kang³⁶, R. Kappert⁵⁹, M. Kavatsyuk⁵⁹, B. C. Ke⁷⁶, I. K. Keshk⁴, A. Khoukaz⁶⁴, P. Kiese³¹, R. Kiuchi¹, R. Kliemt¹², L. Koch³³, O. B. Kolcu^{57A}, B. Kopf⁴, M. Kuemmel⁴, M. Kuessner⁴, A. Kupsc^{40,71}, W. Kühn³³, J. J. Lane⁶², J. S. Lange³³, P. Larin¹⁷, A. Lavania²⁴, L. Lavezzi^{70A,70C}, Z. H. Lei^{67,53}, H. Leithoff³¹, M. Lellmann³¹, T. Lenz³¹, C. Li⁴³, C. Li³⁹, C. H. Li³⁵, Cheng Li^{67,53}, D. M. Li⁷⁶, F. Li^{1,53}, G. Li¹, H. Li⁴⁷, H. Li^{67,53}, H. B. Li^{1,58}, H. J. Li¹⁸, H. N. Li^{51,i}, J. Q. Li⁴, J. S. Li⁵⁴, J. W. Li⁴⁵, Ke Li¹, L. J. Li¹, L. K. Li¹, Lei Li³, M. H. Li³⁹, P. R. Li^{34,j,k}, S. X. Li¹⁰, S. Y. Li⁵⁶, T. Li⁴⁵, W. D. Li^{1,58}, W. G. Li¹, X. H. Li^{67,53}, X. L. Li⁴⁵, Xiaoyu Li^{1,58}, H. Liang^{67,53}, H. Liang³⁰, H. Liang^{1,58}, Y. F. Liang⁴⁹, Y. T. Liang^{28,58}, G. R. Liao¹³, L. Z. Liao⁴⁵, J. Libby²⁴, A. Limphirat⁵⁵, C. X. Lin⁵⁴, D. X. Lin^{28,58}, T. Lin¹, B. J. Liu¹, C. X. Liu¹, D. Liu^{17,67}, F. H. Liu⁴⁸, Fang Liu¹, Feng Liu⁶, G. M. Liu^{51,i}, H. Liu^{34,j,k}, H. B. Liu¹⁴, H. M. Liu^{1,58}, Huanhuan Liu¹, Huihui Liu¹⁹, J. B. Liu^{67,53}, J. L. Liu⁶⁸, J. Y. Liu^{1,58}, K. Liu¹, K. Y. Liu³⁶, Ke Liu²⁰, L. Liu^{67,53}, Lu Liu³⁹, M. H. Liu^{10,f}, P. L. Liu¹, Q. Liu⁵⁸, S. B. Liu^{67,53}, T. Liu^{10,f}, W. K. Liu³⁹, W. M. Liu^{67,53}, X. Liu^{34,j,k}, Y. Liu^{34,j,k}, Y. B. Liu³⁹, Z. A. Liu^{1,53,58}, Z. Q. Liu⁴⁵, X. C. Lou^{1,53,58}, F. X. Lu⁵⁴, H. J. Lu²¹, J. G. Lu^{1,53}, X. L. Lu¹, Y. Lu⁷, Y. P. Lu^{1,53}, Z. H. Lu¹, C. L. Luo³⁷, M. X. Luo⁷⁵, T. Luo^{10,f}, X. L. Luo^{1,53}, X. R. Lyu⁵⁸, Y. F. Lyu³⁹, F. C. Ma³⁶, H. L. Ma¹, L. L. Ma⁴⁵, M. M. Ma^{1,58}, Q. M. Ma¹, R. Q. Ma^{1,58}, R. T. Ma⁵⁸, X. Y. Ma^{1,53}, Y. Ma^{42,g}, F. E. Maas¹⁷, M. Maggiora^{70A,70C}, S. Maldaner⁴, S. Malde⁶⁵, Q. A. Malik⁶⁹, A. Mangoni^{26B}, Y. J. Mao^{42,g}, Z. P. Mao¹, S. Marcello^{70A,70C}, Z. X. Meng⁶¹, J. G. Messchendorp^{59,12}, G. Mezzadri^{27A}, H. Miao¹, T. J. Min³⁸, R. E. Mitchell²⁵, X. H. Mo^{1,53,58}, N. Yu. Muchnoi^{11,b}, H. Muramatsu⁶³, Y. Nefedov³², F. Nerling^{12,d}, I. B. Nikolaev^{11,b}, Z. Ning^{1,53}, S. Nisar^{9,l}, Y. Niu⁴⁵, S. L. Olsen⁵⁸, Q. Ouyang^{1,53,58}, S. Pacetti^{26B,26C}, X. Pan^{10,f}, Y. Pan⁶², A. Pathak³⁰, M. Pelizaeus⁴, H. P. Peng^{67,53}, K. Peters^{12,d}, J. L. Ping³⁷, R. G. Ping^{1,58}, S. Plura³¹, S. Pogodin³², R. Poling⁶³, V. Prasad^{67,53}, F. Z. Qi¹, H. Qi^{67,53}, H. R. Qi⁵⁶, M. Qi³⁸, T. Y. Qi^{10,f}, S. Qian^{1,53}, W. B. Qian⁵⁸, Z. Qian⁵⁴, C. F. Qiao⁵⁸, J. J. Qin⁶⁸, L. Q. Qin¹³, X. P. Qin^{10,f}, X. S. Qin⁴⁵, Z. H. Qin^{1,53}, J. F. Qiu¹, S. Q. Qu³⁹, S. Q. Qu⁵⁶, K. H. Rashid⁶⁹, C. F. Redmer³¹, K. J. Ren³⁵, A. Rivetti^{70C}, V. Rodin⁵⁹, M. Rolo^{70C}, G. Rong^{1,58}, Ch. Rosner¹⁷, S. N. Ruan³⁹, H. S. Sang⁶⁷, A. Sarantsev^{32,c}, Y. Schelhaas³¹, C. Schnier⁴, K. Schoenning⁷¹, M. Scodeggio^{27A,27B}, K. Y. Shan^{10,f}, W. Shan²², X. Y. Shan^{67,53}, J. F. Shanguan⁵⁰, L. G. Shao^{1,58}, M. Shao^{67,53}, C. P. Shen^{10,f}, H. F. Shen^{1,58}, X. Y. Shen^{1,58}, B. A. Shi⁵⁸, H. C. Shi^{67,53}, J. Y. Shi¹, R. S. Shi^{1,58}, X. Shi^{1,53}, X. D. Shi^{67,53}, J. J. Song¹⁸, W. M. Song^{30,1}, Y. X. Song^{42,g}, S. Sosio^{70A,70C}, S. Spataro^{70A,70C}, F. Stieler³¹, K. X. Su⁷², P. P. Su⁵⁰, Y. J. Su⁵⁸, G. X. Sun¹, H. Sun⁵⁸, H. K. Sun¹, J. F. Sun¹⁸, L. Sun⁷², S. S. Sun^{1,58}, T. Sun^{1,58}, W. Y. Sun³⁰, X. Sun^{23,h}, Y. J. Sun^{67,53}, Y. Z. Sun¹, Z. T. Sun⁴⁵, Y. H. Tan⁷²,

Y. X. Tan^{67,53}, C. J. Tang⁴⁹, G. Y. Tang¹, J. Tang⁵⁴, L. Y. Tao⁶⁸, Q. T. Tao^{23,h}, J. X. Teng^{67,53}, V. Thoren⁷¹, W. H. Tian⁴⁷, Y. Tian^{28,58}, I. Uman^{57B}, B. Wang¹, B. L. Wang⁵⁸, C. W. Wang³⁸, D. Y. Wang^{42,g}, F. Wang⁶⁸, H. J. Wang^{34,j,k}, H. P. Wang^{1,58}, K. Wang^{1,53}, L. L. Wang¹, M. Wang⁴⁵, M. Z. Wang^{42,g}, Meng Wang^{1,58}, S. Wang¹³, S. Wang^{10,f}, T. Wang^{10,f}, T. J. Wang³⁹, W. Wang⁵⁴, W. H. Wang⁷², W. P. Wang^{67,53}, X. Wang^{42,g}, X. F. Wang^{34,j,k}, X. L. Wang^{10,f}, Y. D. Wang⁴¹, Y. F. Wang^{1,53,58}, Y. H. Wang⁴³, Y. Q. Wang¹, Yaqian Wang^{16,1}, Z. Wang^{1,53}, Z. Y. Wang^{1,58}, Ziyi Wang⁵⁸, D. H. Wei¹³, F. Weidner⁶⁴, S. P. Wen¹, D. J. White⁶², U. Wiedner⁴, G. Wilkinson⁶⁵, M. Wolke⁷¹, L. Wollenberg⁴, J. F. Wu^{1,58}, L. H. Wu¹, L. J. Wu^{1,58}, X. Wu^{10,f}, X. H. Wu³⁰, Y. Wu⁶⁷, Y. J. Wu²⁸, Z. Wu^{1,53}, L. Xia^{67,53}, T. Xiang^{42,g}, D. Xiao^{34,j,k}, G. Y. Xiao³⁸, H. Xiao^{10,f}, S. Y. Xiao¹, Y. L. Xiao^{10,f}, Z. J. Xiao³⁷, C. Xie³⁸, X. H. Xie^{42,g}, Y. Xie⁴⁵, Y. G. Xie^{1,53}, Y. H. Xie⁶, Z. P. Xie^{67,53}, T. Y. Xing^{1,58}, C. F. Xu¹, C. J. Xu⁵⁴, G. F. Xu¹, H. Y. Xu⁶¹, Q. J. Xu¹⁵, X. P. Xu⁵⁰, Y. C. Xu⁵⁸, Z. P. Xu³⁸, F. Yan^{10,f}, L. Yan^{10,f}, W. B. Yan^{67,53}, W. C. Yan⁷⁶, H. J. Yang^{46,e}, H. L. Yang³⁰, H. X. Yang¹, L. Yang⁴⁷, S. L. Yang⁵⁸, Tao Yang¹, Y. F. Yang³⁹, Y. X. Yang^{1,58}, Yifan Yang^{1,58}, M. Ye^{1,53}, M. H. Ye⁸, J. H. Yin¹, Z. Y. You⁵⁴, B. X. Yu^{1,53,58}, C. X. Yu³⁹, G. Yu^{1,58}, T. Yu⁶⁸, C. Z. Yuan^{1,58}, L. Yuan², S. C. Yuan¹, X. Q. Yuan¹, Y. Yuan^{1,58}, Z. Y. Yuan⁵⁴, C. X. Yue³⁵, A. A. Zafar⁶⁹, F. R. Zeng⁴⁵, X. Zeng Zeng⁶, Y. Zeng^{23,h}, Y. H. Zhan⁵⁴, A. Q. Zhang¹, B. L. Zhang¹, B. X. Zhang¹, D. H. Zhang³⁹, G. Y. Zhang¹⁸, H. Zhang⁶⁷, H. H. Zhang³⁰, H. H. Zhang⁵⁴, H. Y. Zhang^{1,53}, J. L. Zhang⁷³, J. Q. Zhang³⁷, J. W. Zhang^{1,53,58}, J. X. Zhang^{34,j,k}, J. Y. Zhang¹, J. Z. Zhang^{1,58}, Jianyu Zhang^{1,58}, Jiawei Zhang^{1,58}, L. M. Zhang⁵⁶, L. Q. Zhang⁵⁴, Lei Zhang³⁸, P. Zhang¹, Q. Y. Zhang^{35,76}, Shuihan Zhang^{1,58}, Shulei Zhang^{23,h}, X. D. Zhang⁴¹, X. M. Zhang¹, X. Y. Zhang⁴⁵, X. Y. Zhang⁵⁰, Y. Zhang⁶⁵, Y. T. Zhang⁷⁶, Y. H. Zhang^{1,53}, Yan Zhang^{67,53}, Yao Zhang¹, Z. H. Zhang¹, Z. Y. Zhang⁷², Z. Y. Zhang³⁹, G. Zhao¹, J. Zhao³⁵, J. Y. Zhao^{1,58}, J. Z. Zhao^{1,53}, Lei Zhao^{67,53}, Ling Zhao¹, M. G. Zhao³⁹, Q. Zhao¹, S. J. Zhao⁷⁶, Y. B. Zhao^{1,53}, Y. X. Zhao^{28,58}, Z. G. Zhao^{67,53}, A. Zhemchugov^{32,a}, B. Zheng⁶⁸, J. P. Zheng^{1,53}, Y. H. Zheng⁵⁸, B. Zhong³⁷, C. Zhong⁶⁸, X. Zhong⁵⁴, H. Zhou⁴⁵, L. P. Zhou^{1,58}, X. Zhou⁷², X. K. Zhou⁵⁸, X. R. Zhou^{67,53}, X. Y. Zhou³⁵, Y. Z. Zhou^{10,f}, J. Zhu³⁹, K. Zhu¹, K. J. Zhu^{1,53,58}, L. X. Zhu⁵⁸, S. H. Zhu⁶⁶, S. Q. Zhu³⁸, T. J. Zhu⁷³, W. J. Zhu^{10,f}, Y. C. Zhu^{67,53}, Z. A. Zhu^{1,58}, B. S. Zou¹, J. H. Zou¹

(BESIII Collaboration)

¹ *Institute of High Energy Physics, Beijing 100049, People's Republic of China*

² *Beihang University, Beijing 100191, People's Republic of China*

³ *Beijing Institute of Petrochemical Technology, Beijing 102617, People's Republic of China*

⁴ *Bochum Ruhr-University, D-44780 Bochum, Germany*

⁵ *Carnegie Mellon University, Pittsburgh, Pennsylvania 15213, USA*

⁶ *Central China Normal University, Wuhan 430079, People's Republic of China*

⁷ *Central South University, Changsha 410083, People's Republic of China*

⁸ *China Center of Advanced Science and Technology, Beijing 100190, People's Republic of China*

⁹ *COMSATS University Islamabad, Lahore Campus, Defence Road, Off Raiwind Road, 54000 Lahore, Pakistan*

¹⁰ *Fudan University, Shanghai 200433, People's Republic of China*

¹¹ *G.I. Budker Institute of Nuclear Physics SB RAS (BINP), Novosibirsk 630090, Russia*

¹² *GSI Helmholtzcentre for Heavy Ion Research GmbH, D-64291 Darmstadt, Germany*

¹³ *Guangxi Normal University, Guilin 541004, People's Republic of China*

¹⁴ *Guangxi University, Nanning 530004, People's Republic of China*

¹⁵ *Hangzhou Normal University, Hangzhou 310036, People's Republic of China*

¹⁶ *Hebei University, Baoding 071002, People's Republic of China*

¹⁷ *Helmholtz Institute Mainz, Staudinger Weg 18, D-55099 Mainz, Germany*

¹⁸ *Henan Normal University, Xinxiang 453007, People's Republic of China*

¹⁹ *Henan University of Science and Technology, Luoyang 471003, People's Republic of China*

²⁰ *Henan University of Technology, Zhengzhou 450001, People's Republic of China*

²¹ *Huangshan College, Huangshan 245000, People's Republic of China*

²² *Hunan Normal University, Changsha 410081, People's Republic of China*

²³ *Hunan University, Changsha 410082, People's Republic of China*

²⁴ *Indian Institute of Technology Madras, Chennai 600036, India*

²⁵ *Indiana University, Bloomington, Indiana 47405, USA*

²⁶ *INFN Laboratori Nazionali di Frascati, (A)INFN Laboratori Nazionali di Frascati, I-00044, Frascati, Italy;*

- (B)INFN Sezione di Perugia, I-06100, Perugia, Italy; (C)University of Perugia, I-06100, Perugia, Italy
- ²⁷ INFN Sezione di Ferrara, (A)INFN Sezione di Ferrara, I-44122, Ferrara, Italy; (B)University of Ferrara, I-44122, Ferrara, Italy
- ²⁸ Institute of Modern Physics, Lanzhou 730000, People's Republic of China
- ²⁹ Institute of Physics and Technology, Peace Avenue 54B, Ulaanbaatar 13330, Mongolia
- ³⁰ Jilin University, Changchun 130012, People's Republic of China
- ³¹ Johannes Gutenberg University of Mainz, Johann-Joachim-Becher-Weg 45, D-55099 Mainz, Germany
- ³² Joint Institute for Nuclear Research, 141980 Dubna, Moscow region, Russia
- ³³ Justus-Liebig-Universitaet Giessen, II. Physikalisches Institut, Heinrich-Buff-Ring 16, D-35392 Giessen, Germany
- ³⁴ Lanzhou University, Lanzhou 730000, People's Republic of China
- ³⁵ Liaoning Normal University, Dalian 116029, People's Republic of China
- ³⁶ Liaoning University, Shenyang 110036, People's Republic of China
- ³⁷ Nanjing Normal University, Nanjing 210023, People's Republic of China
- ³⁸ Nanjing University, Nanjing 210093, People's Republic of China
- ³⁹ Nankai University, Tianjin 300071, People's Republic of China
- ⁴⁰ National Centre for Nuclear Research, Warsaw 02-093, Poland
- ⁴¹ North China Electric Power University, Beijing 102206, People's Republic of China
- ⁴² Peking University, Beijing 100871, People's Republic of China
- ⁴³ Qufu Normal University, Qufu 273165, People's Republic of China
- ⁴⁴ Shandong Normal University, Jinan 250014, People's Republic of China
- ⁴⁵ Shandong University, Jinan 250100, People's Republic of China
- ⁴⁶ Shanghai Jiao Tong University, Shanghai 200240, People's Republic of China
- ⁴⁷ Shanxi Normal University, Linfen 041004, People's Republic of China
- ⁴⁸ Shanxi University, Taiyuan 030006, People's Republic of China
- ⁴⁹ Sichuan University, Chengdu 610064, People's Republic of China
- ⁵⁰ Soochow University, Suzhou 215006, People's Republic of China
- ⁵¹ South China Normal University, Guangzhou 510006, People's Republic of China
- ⁵² Southeast University, Nanjing 211100, People's Republic of China
- ⁵³ State Key Laboratory of Particle Detection and Electronics, Beijing 100049, Hefei 230026, People's Republic of China
- ⁵⁴ Sun Yat-Sen University, Guangzhou 510275, People's Republic of China
- ⁵⁵ Suranaree University of Technology, University Avenue 111, Nakhon Ratchasima 30000, Thailand
- ⁵⁶ Tsinghua University, Beijing 100084, People's Republic of China
- ⁵⁷ Turkish Accelerator Center Particle Factory Group, (A)Istinye University, 34010, Istanbul, Turkey; (B)Near East University, Nicosia, North Cyprus, Mersin 10, Turkey
- ⁵⁸ University of Chinese Academy of Sciences, Beijing 100049, People's Republic of China
- ⁵⁹ University of Groningen, NL-9747 AA Groningen, The Netherlands
- ⁶⁰ University of Hawaii, Honolulu, Hawaii 96822, USA
- ⁶¹ University of Jinan, Jinan 250022, People's Republic of China
- ⁶² University of Manchester, Oxford Road, Manchester, M13 9PL, United Kingdom
- ⁶³ University of Minnesota, Minneapolis, Minnesota 55455, USA
- ⁶⁴ University of Muenster, Wilhelm-Klemm-Strasse 9, 48149 Muenster, Germany
- ⁶⁵ University of Oxford, Keble Road, Oxford OX13RH, United Kingdom
- ⁶⁶ University of Science and Technology Liaoning, Anshan 114051, People's Republic of China
- ⁶⁷ University of Science and Technology of China, Hefei 230026, People's Republic of China
- ⁶⁸ University of South China, Hengyang 421001, People's Republic of China
- ⁶⁹ University of the Punjab, Lahore-54590, Pakistan
- ⁷⁰ University of Turin and INFN, (A)University of Turin, I-10125, Turin, Italy; (B)University of Eastern Piedmont, I-15121, Alessandria, Italy; (C)INFN, I-10125, Turin, Italy
- ⁷¹ Uppsala University, Box 516, SE-75120 Uppsala, Sweden
- ⁷² Wuhan University, Wuhan 430072, People's Republic of China

⁷³ Xinyang Normal University, Xinyang 464000, People's Republic of China

⁷⁴ Yunnan University, Kunming 650500, People's Republic of China

⁷⁵ Zhejiang University, Hangzhou 310027, People's Republic of China

⁷⁶ Zhengzhou University, Zhengzhou 450001, People's Republic of China

^a Also at the Moscow Institute of Physics and Technology, Moscow 141700, Russia

^b Also at the Novosibirsk State University, Novosibirsk, 630090, Russia

^c Also at the NRC "Kurchatov Institute", PNPI, 188300, Gatchina, Russia

^d Also at Goethe University Frankfurt, 60323 Frankfurt am Main, Germany

^e Also at Key Laboratory for Particle Physics, Astrophysics and Cosmology, Ministry of Education; Shanghai Key Laboratory for Particle Physics and Cosmology; Institute of Nuclear and Particle Physics, Shanghai 200240, People's Republic of China

^f Also at Key Laboratory of Nuclear Physics and Ion-beam Application (MOE) and Institute of Modern Physics, Fudan University, Shanghai 200443, People's Republic of China

^g Also at State Key Laboratory of Nuclear Physics and Technology, Peking University, Beijing 100871, People's Republic of China

^h Also at School of Physics and Electronics, Hunan University, Changsha 410082, China

ⁱ Also at Guangdong Provincial Key Laboratory of Nuclear Science, Institute of Quantum Matter, South China Normal University, Guangzhou 510006, China

^j Also at Frontiers Science Center for Rare Isotopes, Lanzhou University, Lanzhou 730000, People's Republic of China

^k Also at Lanzhou Center for Theoretical Physics, Lanzhou University, Lanzhou 730000, People's Republic of China

^l Also at the Department of Mathematical Sciences, IBA, Karachi, Pakistan

By analyzing e^+e^- annihilation data with an integrated luminosity of 2.93 fb^{-1} collected at the center-of-mass energy $\sqrt{s} = 3.773 \text{ GeV}$ with the BESIII detector, we present the first absolute measurements of the branching fractions of twenty Cabibbo-suppressed hadronic $D^{0(+)}$ decays involving multiple pions. The largest four branching fractions obtained are $\mathcal{B}(D^0 \rightarrow \pi^+\pi^-\pi^0) = (1.343 \pm 0.013_{\text{stat}} \pm 0.016_{\text{syst}})\%$, $\mathcal{B}(D^0 \rightarrow \pi^+\pi^-2\pi^0) = (0.998 \pm 0.019_{\text{stat}} \pm 0.024_{\text{syst}})\%$, $\mathcal{B}(D^+ \rightarrow 2\pi^+\pi^-\pi^0) = (1.174 \pm 0.021_{\text{stat}} \pm 0.021_{\text{syst}})\%$, and $\mathcal{B}(D^+ \rightarrow 2\pi^+\pi^-2\pi^0) = (1.074 \pm 0.040_{\text{stat}} \pm 0.030_{\text{syst}})\%$. The CP asymmetries for the six decays with highest event yields are also determined.

Investigations of hadronic $D^{0(+)}$ decays are of general importance for both charm and bottom physics. For example, Ref. [1] suggests that hadronic $D^{0(+)}$ decays involving three charged pions are crucial backgrounds for the tests of lepton flavor universality (LFU) in semileptonic B decays. However, many Cabibbo-suppressed hadronic $D^{0(+)}$ decays with three charged pions are unexplored mainly due to low detection efficiencies and high background contamination. Precision and comprehensive measurements of the absolute branching fractions (BFs) of these decays provide necessary inputs to unravel the hints of LFU violation observed in semileptonic B decays.

According to theoretical predictions, the CP violation in charmed hadron decays is expected to be at the order of 10^{-3} for singly Cabibbo-suppressed processes, and much smaller for Cabibbo-favored and doubly Cabibbo-suppressed processes [2–9]. The LHCb experiment reported the first observation of CP violation in $D^0 \rightarrow K^+K^-$ and $\pi^+\pi^-$ with an asymmetry difference of $\Delta A_{CP} = (1.54 \pm 0.29) \times 10^{-3}$ [10]. A similar magnitude of CP asymmetry is predicted in $D^0 \rightarrow K^+K^{*-}$ and $D^0 \rightarrow \rho^+\pi^-$ [8]. Refs. [2, 3] suggest that the CP

asymmetries in $D \rightarrow \rho\pi$ decays are in the range of $(0.3 \sim 5) \times 10^{-4}$. Therefore, searching for CP violation in Cabibbo-suppressed $D^{0(+)}$ decays into three pions is an interesting pursuit.

The Cabibbo-suppressed hadronic neutral D decays into $\pi^+\pi^-\pi^0$ and $\pi^+\pi^-\pi^0\pi^0$ also provide a promising way to extract the CKM angle γ in $B^+ \rightarrow D^{(*)0}K^{(*)+}$ due to the similar magnitude of interference amplitudes between D^0 and \bar{D}^0 decays into $\pi^+\pi^-\pi^0$, $\pi^+\pi^-\pi^0\pi^0$ [11]. More precise measurements of these BFs can improve estimations of the measurement precision for the CP violation phase angle γ with these modes.

This Letter reports the first absolute measurements of the BFs of the Cabibbo-suppressed hadronic decays $D^0 \rightarrow \pi^+\pi^-\pi^0$, $\pi^+\pi^-2\pi^0$, $\pi^+\pi^-2\eta$, $4\pi^0$, $3\pi^0\eta$, $2\pi^+2\pi^-\pi^0$, $2\pi^+2\pi^-\eta$, $\pi^+\pi^-3\pi^0$, $2\pi^+2\pi^-2\pi^0$, and $D^+ \rightarrow 2\pi^+\pi^-$, $\pi^+2\pi^0$, $2\pi^+\pi^-\pi^0$, $\pi^+3\pi^0$, $3\pi^+2\pi^-$, $2\pi^+\pi^-2\pi^0$, $2\pi^+\pi^-\pi^0\eta$, $\pi^+4\pi^0$, $\pi^+3\pi^0\eta$, $3\pi^+2\pi^-\pi^0$, $2\pi^+\pi^-3\pi^0$ based on 2.93 fb^{-1} e^+e^- annihilation data taken at the center-of-mass energy $\sqrt{s} = 3.773 \text{ GeV}$ with the BESIII detector [12]. Moreover, CP asymmetries for the six decays with the highest yields are determined. To date, only the BFs of seven of these decay modes

have been measured relative to reference modes and only the CP asymmetries in $D^0(\bar{D}^0) \rightarrow \pi^+\pi^-\pi^0$ and $D^\pm \rightarrow \pi^+\pi^-\pi^\pm$ have been measured by various experiments [13]. Throughout this Letter, charge-conjugated processes are implied except when discussing CP asymmetries.

The BESIII detector is a magnetic spectrometer [14] located at the Beijing Electron Positron Collider (BEPCII) [15]. Simulated samples produced with a GEANT4-based [16] Monte Carlo (MC) package including the geometric description of the BESIII detector and the detector response, are used to determine the detection efficiencies and to estimate backgrounds. The simulation of e^+e^- annihilations modeled with the generator KKMC [17] includes the beam-energy spread and initial-state radiation. The inclusive MC samples consist of the production of $D\bar{D}$ pairs with consideration of quantum coherence for all neutral D modes, the non- $D\bar{D}$ decays of the $\psi(3770)$, the initial-state radiation production of the J/ψ and $\psi(3686)$ states, and continuum processes. Known decay modes are modeled with EVTGEN [18] using the BFs taken from Ref. [13], and the remaining unknown decays of the charmonium states are modeled with LUNDCHARM [19, 20]. Final-state radiation from charged final-state particles is incorporated using PHOTOS [21].

At $\sqrt{s} = 3.773$ GeV, $D^0\bar{D}^0$ or D^+D^- pairs are produced without accompanying hadron(s), thereby offering a clean environment to investigate hadronic D decays with double-tag (DT) method [22]. The single-tag (ST) \bar{D} candidates are selected by reconstructing a \bar{D}^0 or D^- in the hadronic decay modes: $\bar{D}^0 \rightarrow K^+\pi^-$, $K^+\pi^-\pi^0$, and $K^+\pi^-\pi^-\pi^+$, and $D^- \rightarrow K^+\pi^-\pi^-$, $K_S^0\pi^-$, $K^+\pi^-\pi^-\pi^0$, $K_S^0\pi^-\pi^0$, $K_S^0\pi^+\pi^-\pi^-$, and $K^+K^-\pi^-$. Events in which a signal candidate is reconstructed in the presence of an ST \bar{D} meson are referred to as DT events. The BF of the signal decay is determined by [23]

$$\mathcal{B}_{\text{sig}} = N_{\text{DT}} / (N_{\text{ST}}^{\text{tot}} \cdot \epsilon_{\text{sig}}), \quad (1)$$

where $N_{\text{ST}}^{\text{tot}} = \sum_i N_{\text{ST}}^i$ and N_{DT} are the total yields of the ST and DT candidates in data, respectively. The ST yield for the tag mode i is N_{ST}^i , and the efficiency ϵ_{sig} for detecting the signal D decay is averaged over the tag modes i .

The selection criteria of K^\pm , π^\pm , K_S^0 , π^0 , and η , are the same as those used in the analyses presented in Refs. [23, 24]. For $\bar{D}^0 \rightarrow K^+\pi^-$, the backgrounds from cosmic rays and Bhabha events are rejected by using the same requirements described in Ref. [25]. For $\bar{D}^0 \rightarrow K^+\pi^-\pi^-\pi^+$, the $\bar{D}^0 \rightarrow K_S^0K^\pm\pi^\mp$ decays are suppressed by requiring the invariant masses of all $\pi^+\pi^-$ pairs to be outside the mass window (0.483, 0.513) GeV/ c^2 .

Tagged \bar{D} mesons are identified using two variables: the energy difference $\Delta E_{\text{tag}} \equiv E_{\text{tag}} - E_b$ and the beam-constrained mass $M_{\text{BC}}^{\text{tag}} \equiv \sqrt{E_b^2 - |\vec{p}_{\text{tag}}|^2}$. Here, E_b

is the beam energy, \vec{p}_{tag} and E_{tag} are the momentum and energy of \bar{D} in the rest frame of e^+e^- system, respectively. The ΔE_{tag} of ST \bar{D} candidates must be in the range $(-55, 40)$ MeV for the tag modes involving π^0 and $(-25, 25)$ MeV for the other tag modes, due to differing resolutions. For each tag mode, if there are multiple candidates in an event, only the one yielding the smallest $|\Delta E_{\text{tag}}|$ is accepted.

To extract the yields of ST \bar{D} candidates for individual tag modes, binned maximum-likelihood fits are performed to the corresponding $M_{\text{BC}}^{\text{tag}}$ distributions of the accepted ST candidates following Ref. [24]. The \bar{D} signal is modeled by an MC-simulated shape convolved with a double-Gaussian function describing the resolution difference between the data and MC simulation. The combinatorial background shape is described by an ARGUS function [26]. The total yields of the ST \bar{D}^0 and D^- candidates in data are $(232.8 \pm 0.2_{\text{stat}}) \times 10^4$ and $(155.8 \pm 0.2_{\text{stat}}) \times 10^4$, respectively.

The signal D decays are selected from the remaining tracks and showers recoiling against the tagged \bar{D} candidates. To reject the main backgrounds from Cabibbo-suppressed decays containing K_S^0 , the $\pi^+\pi^-$ and $\pi^0\pi^0$ combinations are required to not fall in the mass windows (0.468, 0.528) GeV/ c^2 and (0.428, 0.548) GeV/ c^2 , respectively. These mass windows correspond to at least 4σ of resolution.

Signal D mesons are identified using the energy difference ΔE_{sig} and the beam-constrained mass $M_{\text{BC}}^{\text{sig}}$, calculated similarly to the ST side. For each signal mode, if there are multiple candidates in an event, only the one with the minimum $|\Delta E_{\text{sig}}|$ is chosen. Signal decays are required to satisfy the ΔE_{sig} requirements shown in Table 1.

For each signal decay mode, the signal yield (N_{DT}) is obtained from a two-dimensional (2D) unbinned maximum-likelihood fit [27] to the $M_{\text{BC}}^{\text{tag}}$ versus $M_{\text{BC}}^{\text{sig}}$ distribution of the accepted DT candidates. See Fig. 2 in the Supplemental Material [28] for an illustration of the 2D distribution. The signal events concentrate around $M_{\text{BC}}^{\text{tag}} = M_{\text{BC}}^{\text{sig}} = M_D$, where M_D is the averaged mass of D [13]. The events with correctly reconstructed D (\bar{D}) and incorrectly reconstructed \bar{D} (D), referred to as BKGI, spread along the lines around $M_{\text{BC}}^{\text{sig}} = M_D$ ($M_{\text{BC}}^{\text{tag}} = M_D$). Events smeared along the diagonal (BKGII) are mainly from the $e^+e^- \rightarrow q\bar{q}$ processes. Events with uncorrelated and incorrectly reconstructed D and \bar{D} (BKGIII) disperse across the whole allowed kinematic region.

In the fit, the probability density functions (PDFs) for signal, BKGI, BKGII, and BKGIII contributions are constructed as $a(x, y)$, $b_x(x) \cdot c_y(y; M_{\text{BC}}^{\text{end}}, \xi_y) + b_y(y) \cdot c_x(x; M_{\text{BC}}^{\text{end}}, \xi_x)$, $c_z(z; \sqrt{2}M_{\text{BC}}^{\text{end}}, \xi_z) \cdot g(k; 0, \sigma_k)$, and $c_x(x; M_{\text{BC}}^{\text{end}}, \xi_x) \cdot c_y(y; M_{\text{BC}}^{\text{end}}, \xi_y)$, respectively. Here, $x = M_{\text{BC}}^{\text{sig}}$, $y = M_{\text{BC}}^{\text{tag}}$, $z = (x + y)/\sqrt{2}$, and $k = (x -$

$y)/\sqrt{2}$. The PDFs of signal, $a(x, y)$, $b_x(x)$, and $b_y(y)$, are described by the MC-simulated shapes smeared with individual Gaussian resolution function with parameters derived from the corresponding one-dimensional M_{BC} fits, to consider resolution difference between data and MC simulation. $c_f(f; M_{\text{BC}}^{\text{end}}, \xi_f)$ is an ARGUS function [26] (f denotes x , y , or z), where the endpoint $M_{\text{BC}}^{\text{end}} = 1.8865 \text{ GeV}/c^2$ is fixed in the fit. The Gaussian function $g(k; 0, \sigma_k)$ has a mean of zero and a standard deviation parameterized by $\sigma_k = \sigma_0 \cdot (\sqrt{2}M_{\text{BC}}^{\text{end}} - z)^p$, where σ_0 and p are fit parameters. In addition, the yields and shapes of the peaking background (PBKG) components, which are mainly from D decays into the same final state as a signal mode but involve $K_S^0 \rightarrow \pi^+\pi^-$ or $\pi^0\pi^0$ and $K^- \rightarrow \pi^-\pi^0$ decay, are fixed based on MC simulations and the known BF's of various PBKG components [13, 29]. Relative to the corresponding signal yields, the PBKG components are 9.5%, 18.2%, and 36.2% for $D^+ \rightarrow \pi^+4\pi^0$, $D^0 \rightarrow 2\pi^+2\pi^-\pi^0$, and $D^0 \rightarrow \pi^+\pi^-3\pi^0$, respectively, and range from 0.1% to 6.3% for the other signal decays.

The $M_{\text{BC}}^{\text{tag}}$ and $M_{\text{BC}}^{\text{sig}}$ projections of the 2D fits of the DT candidates reconstructed from data are shown in Fig. 1 and the fitted DT yields are summarized in Table 1.

To determine the signal efficiencies (ϵ_{sig}), the three-body decays are simulated with a modified data-driven generator BODY3 [18], which was developed to simulate different intermediate states in data for a given three-body final state. The Dalitz plot from data, corrected for backgrounds and efficiencies, is taken as input for the BODY3 generator. The efficiencies across phase space are obtained with MC samples generated according to a phase space distribution. Each of the four-body and five-body decays is simulated with a mixed signal MC sample. These decays generated with phase space models including contributions from η , ω , η' , $\rho(770)$, $a_0(980)$, $a_1(1260)$, $b_1(1235)$ and ϕ intermediate states are mixed with fractions obtained by examining the corresponding invariant mass spectra. The data distributions for momenta and $\cos\theta$ (where θ is the polar angle of particle in the e^+e^- rest frame) of the daughter particles, and the invariant masses of each of the two- and multi-body particle combinations agree with the MC simulations. See Figs. 3-11 in the Supplemental Material [28] for explicit comparisons.

The results for N_{DT} , ϵ_{sig} , and the extracted BF's are summarized in Table 1. The smallest statistical significance is 6.8 standard deviations for $D^+ \rightarrow \pi^+4\pi^0$ mode. The signal efficiencies have been corrected by the data-MC differences in the selection efficiencies of π^\pm tracking, particle identification (PID) procedures and the reconstruction of π^0 or η .

The systematic uncertainties relative to the obtained BF's are discussed below. In the BF determinations using Eq. (1), all uncertainties from selecting the ST \bar{D} candidates are cancelled in the ratio. Systematic

uncertainties in the total yields of ST \bar{D} mesons related to the $M_{\text{BC}}^{\text{tag}}$ fits to the ST \bar{D} candidates, were previously estimated to be 0.5% for both neutral and charged \bar{D} [30–32].

The tracking and PID efficiencies of π^\pm are investigated using other DT $D\bar{D}$ hadronic events. The differences of efficiencies between data and MC simulations are weighted by the corresponding π^\pm momentum spectra of signal MC events. The systematic uncertainties due to tracking and PID are assigned to be (0.2-0.4)% per π^\pm , based on the residual statistical uncertainties of the measured data-MC differences.

The systematic uncertainty of the π^0 reconstruction is assigned as (0.4-0.9)% per π^0 from studies of DT $D\bar{D}$ hadronic decay samples of $D^0 \rightarrow K^-\pi^+$, $K^-\pi^+\pi^+\pi^-$ versus $\bar{D}^0 \rightarrow K^+\pi^-\pi^0$, $K_S^0\pi^0$ [30, 31]. Due to limited η statistics, the systematic uncertainty for η reconstruction is assigned by referring to that of π^0 .

The systematic uncertainty in the 2D fit to the $M_{\text{BC}}^{\text{tag}}$ versus $M_{\text{BC}}^{\text{sig}}$ distribution is examined by varying the smeared Gaussian function ($\pm 1\sigma$), the endpoint of the ARGUS function ($\pm 0.2 \text{ MeV}/c^2$), and the fixed PBKG yields ($\pm 1\sigma$ of the quoted BF). Adding the changes from these three sources in quadrature yields the corresponding systematic uncertainties.

The systematic uncertainty due to the ΔE_{sig} requirement ranges from (0.1-1.3)% depending on the signal mode. They are evaluated from the efficiency differences obtained with and without smearing the ΔE_{sig} distributions for signal MC events with parameters derived from $D^0 \rightarrow \pi^+\pi^-\pi^0$, $D^0 \rightarrow \pi^+\pi^-2\pi^0$, $D^+ \rightarrow \pi^+2\pi^0$, and $D^+ \rightarrow 2\pi^+\pi^-\pi^0$ to get the data-MC differences.

The systematic uncertainty due to the BODY3 generator is considered by varying the number of bins by $\pm 20\%$ and the systematic uncertainty in the mixed MC model is assigned by varying the fractions of various components by $\pm 1\sigma$ of the quoted BF, when available. Unmeasured components are varied by $\pm 25\%$, beyond which comparisons with observed mass spectra are unsatisfactory. The largest change of the signal efficiencies, (0.2-5.7)% for various signal modes, are assigned as the corresponding systematic uncertainties.

The systematic uncertainties due to the mass window applied to reject K_S^0 events are crosschecked by examining the changes of the BF's by varying the corresponding boundaries of the window by $\pm 5 \text{ MeV}/c^2$. If the difference of the BF is larger than 1 time the statistical uncertainty on the difference (taking the correlated samples into account), it is assigned as the corresponding systematic uncertainty. Otherwise, it is neglected.

The measurements of the BF's of the neutral D decays are affected by quantum correlation effect [33]. To take this effect into account, the CP -even fractions in various decays are needed. The $D^0 \rightarrow 4\pi^0$ and $D^0 \rightarrow 3\pi^0\eta$ final

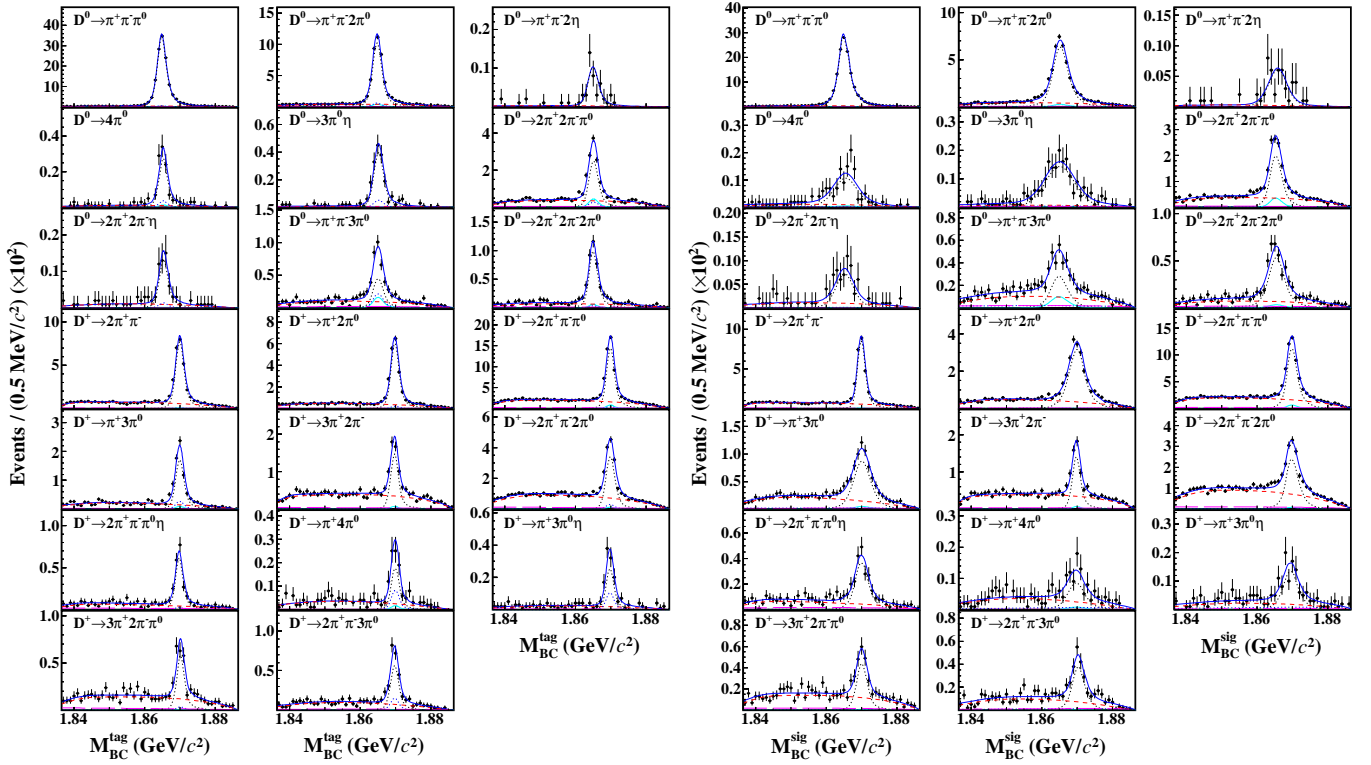


Fig. 1. Projections of M_{BC}^{tag} (left) and M_{BC}^{sig} (right) of the 2D fits to the DT candidate events. Points with error bars are data and blue solid curves are the fit results. Black dotted, cyan blue solid, blue dotted, red dotted, pink long-dashed correspond to fitted signal, fixed peaking background, BKGI, BKGII, and BKGIII components, respectively.

states are both CP -even eigenstates. For $D^0 \rightarrow \pi^+ \pi^- \pi^0$, its CP -even fraction has been determined to be 0.973 ± 0.017 [5]. For $D^0 \rightarrow \pi^+ \pi^- 2\pi^0$, $D^0 \rightarrow 2\pi^+ 2\pi^- \pi^0$, $D^0 \rightarrow \pi^+ \pi^- 3\pi^0$, and $D^0 \rightarrow 2\pi^+ 2\pi^- 2\pi^0$, the CP -even fractions are estimated by the CP -even tag $D^0 \rightarrow K^+ K^-$ and the CP -odd tag $D^0 \rightarrow K_S^0 \pi^0$. Using the same method as described in Ref. [1] and the necessary parameters quoted from Refs. [2–4], we obtain the correction factors to account for the quantum correlation effect on the measured BF; the results are summarized in Table 3 of the Supplemental Material [28]. After correcting the signal efficiencies by the individual factors, the residual uncertainties are assigned as systematic uncertainties.

The uncertainties of MC statistics for various signal decays, (0.2-1.3)%, are considered as a systematic uncertainty. The uncertainties of the daughter BFs of $\eta \rightarrow \gamma\gamma$ and $\pi^0 \rightarrow \gamma\gamma$ are 0.51% and 0.03%, respectively [13].

Adding all individual effects for each signal decay quadratically yields the total systematic uncertainties to be (1.2-11.9)% depending on the signal mode. The detailed systematic uncertainties are given in Table 5 of the Supplemental Material [28].

For the six decay modes with the highest yields, the BFs of D and \bar{D} decays, $\mathcal{B}_{\text{sig}}^+$ and $\mathcal{B}_{\text{sig}}^-$, are measured separately. Their asymmetry is determined

by $\mathcal{A}_{CP}^{\text{sig}} = \frac{\mathcal{B}_{\text{sig}}^+ - \mathcal{B}_{\text{sig}}^-}{\mathcal{B}_{\text{sig}}^+ + \mathcal{B}_{\text{sig}}^-}$. The obtained BFs and asymmetries are summarized in Table 2. We find no statistically significant CP violation. Several systematic uncertainties cancel in the asymmetry: the tracking and PID of $\pi^+ \pi^-$ pairs, π^0 and η reconstruction, daughter BFs, K_S^0 rejection windows, MC modeling, and strong phase of D^0 decays. The other systematic uncertainties are estimated separately as above.

To summarize, by analyzing 2.93 fb^{-1} of $e^+ e^-$ annihilation data recorded at $\sqrt{s} = 3.773 \text{ GeV}$ with the BESIII detector, we present the first absolute measurements of the BFs of twenty Cabibbo-suppressed hadronic $D^{0(+)}$ decays involving multiple pions. For $D^0 \rightarrow \pi^+ \pi^- \pi^0$, $\pi^+ \pi^- 2\pi^0$, $2\pi^+ 2\pi^- \pi^0$, and $D^+ \rightarrow 2\pi^+ \pi^-$, $\pi^+ 2\pi^0$, $2\pi^+ \pi^- \pi^0$, $3\pi^+ 2\pi^-$, the BF precisions are improved by factors of 1.2-2.9 compared to the world average values based on relative measurements. For the other 13 decay modes, the BFs are measured for the first time. The reported BFs offer important input for reliable estimations of potential background sources in the precision measurements of B and D decays, especially to properly evaluate the tensions found in the LFU tests with semileptonic B decays. Amplitude analyses of these multi-body decays with larger data samples available in the near future [39, 40] will open

Table 1. Requirements of ΔE_{sig} , DT yields in data (N_{DT}), detection efficiencies (ϵ_{sig} , including the BF's of η , and π^0 as well as correction factors described later), and the obtained BF's (\mathcal{B}_{sig}). The first nine modes are D^0 decays and the others are D^+ decays. For \mathcal{B}_{sig} , numbers in the first and second parentheses are last two digits of the statistical and systematic uncertainties, respectively. For N_{DT} , uncertainties are statistical only.

Decay	ΔE_{sig} (MeV)	N_{DT}	ϵ_{sig} (%)	\mathcal{B}_{sig} ($\times 10^{-4}$)
$\pi^+\pi^-\pi^0$	(-62, 36)	12792.6(120.1)	40.91	134.3(13)(16)
$\pi^+\pi^-2\pi^0$	(-75, 37)	3783.7(70.5)	16.29	99.8(19)(24)
$\pi^+\pi^-2\eta$	(-37, 29)	42.5(6.7)	2.14	8.5(13)(04)
$4\pi^0$	(-105, 41)	96.0(11.5)	5.41	7.6(09)(07)
$3\pi^0\eta$	(-82, 40)	155.3(14.7)	2.83	23.6(22)(17)
$2\pi^+2\pi^-\pi^0$	(-52, 33)	942.4(40.0)	11.70	34.6(15)(15)
$2\pi^+2\pi^-\eta$	(-36, 28)	48.5(7.8)	3.46	6.0(10)(06)
$\pi^+\pi^-3\pi^0$	(-76, 39)	182.7(20.9)	5.13	15.3(17)(13)
$2\pi^+2\pi^-2\pi^0$	(-64, 36)	350.0(22.9)	3.15	47.7(31)(21)
$2\pi^+\pi^-$	(-30, 28)	2614.3(58.0)	50.63	33.1(07)(05)
$\pi^+2\pi^0$	(-96, 44)	1968.0(51.7)	27.33	46.2(12)(09)
$2\pi^+\pi^-\pi^0$	(-59, 35)	4649.5(83.5)	25.42	117.4(21)(21)
$\pi^+3\pi^0$	(-86, 39)	573.7(30.2)	8.83	41.7(22)(13)
$3\pi^+2\pi^-$	(-37, 33)	462.1(28.7)	16.26	18.2(11)(10)
$2\pi^+\pi^-2\pi^0$	(-74, 39)	1207.1(45.4)	7.21	107.4(40)(30)
$2\pi^+\pi^-\pi^0\eta$	(-51, 33)	191.4(15.9)	3.17	38.8(32)(12)
$\pi^+4\pi^0$	(-90, 41)	56.7(10.4)	1.87	19.5(36)(23)
$\pi^+3\pi^0\eta$	(-66, 37)	79.7(10.9)	1.77	28.9(40)(22)
$3\pi^+2\pi^-\pi^0$	(-49, 34)	182.8(17.3)	5.02	23.4(22)(15)
$2\pi^+\pi^-3\pi^0$	(-66, 37)	185.9(17.0)	3.49	34.2(31)(16)

Table 2. Charge-separated BF's ($\mathcal{B}_{\text{sig}}^+$ and $\mathcal{B}_{\text{sig}}^-$), and their asymmetries ($\mathcal{A}_{CP}^{\text{sig}}$). The first and second uncertainties are statistical and systematic, respectively, for $\mathcal{A}_{CP}^{\text{sig}}$; while uncertainties for $\mathcal{B}_{\text{sig}}^+$ and $\mathcal{B}_{\text{sig}}^-$ are only statistical.

Decay	$\mathcal{B}_{\text{sig}}^+(\times 10^{-4})$	$\mathcal{B}_{\text{sig}}^-(\times 10^{-4})$	$\mathcal{A}_{CP}^{\text{sig}}$ (%)
$\pi^+\pi^-\pi^0$	134.8 ± 1.8	133.3 ± 1.8	$+0.6 \pm 0.9 \pm 0.4$
$\pi^+\pi^-2\pi^0$	97.1 ± 2.6	102.3 ± 2.7	$-2.6 \pm 1.9 \pm 0.7$
$2\pi^+\pi^-$	33.5 ± 1.0	32.7 ± 1.0	$+1.2 \pm 2.1 \pm 0.6$
$\pi^+2\pi^0$	48.9 ± 1.8	43.4 ± 1.7	$+6.0 \pm 2.7 \pm 0.5$
$2\pi^+\pi^-\pi^0$	117.7 ± 3.0	116.8 ± 3.0	$+0.4 \pm 1.8 \pm 0.8$
$2\pi^+\pi^-2\pi^0$	102.7 ± 5.6	111.6 ± 5.8	$-4.2 \pm 3.8 \pm 1.3$

an opportunity to precisely extract more quasi-two-body hadronic $D^{0(+)}$ decay rates, e.g. $D^+ \rightarrow \rho^+\pi^0$. Detailed knowledge of these hadronic $D^{0(+)}$ decays is essential to deeply explore quark U-spin and SU(3)-flavor symmetry breaking effects and thereby improve the predictions of CP violation in the charm sector [2, 41, 42]. Additionally, the asymmetries of the charge-conjugated BF's of the six

$D^{0(+)}$ decays with largest yields are determined. No statistically significant CP violation is observed.

The BESIII collaboration thanks the staff of BEPCII and the IHEP computing center for their strong support. This work is supported in part by National Key R&D Program of China under Contracts Nos. 2020YFA0406400 and 2020YFA0406300; National Natural Science Foundation of China (NSFC) under Contracts Nos. 11625523, 11635010, 11735014, 11822506, 11835012, 11935015, 11935016, 11935018, 11961141012, 12022510, 12025502, 12035009, 12035013, 12061131003, 12192260, 12192261, 12192262, 12192263, 12192264, 12192265; the Chinese Academy of Sciences (CAS) Large-Scale Scientific Facility Program; Joint Large-Scale Scientific Facility Funds of the NSFC and CAS under Contracts Nos. U1732263, U1832207, U1932102; CAS Key Research Program of Frontier Sciences under Contract No. QYZDJ-SSW-SLH040; 100 Talents Program of CAS; INPAC and Shanghai Key Laboratory for Particle Physics and Cosmology; ERC under Contract No. 758462; European Union Horizon 2020 research and innovation programme under Contract No. Marie Skłodowska-Curie grant agreement No 894790; German Research Foundation DFG under Contracts Nos. 443159800, Collaborative Research Center CRC 1044, FOR 2359, FOR 2359, GRK 2149; Istituto Nazionale di Fisica Nucleare, Italy; Ministry of Development of Turkey under Contract No. DPT2006K-120470; National Science and Technology fund; Olle Engkvist Foundation under Contract No. 200-0605; STFC (United Kingdom); The Knut and Alice Wallenberg Foundation (Sweden) under Contract No. 2016.0157; The Royal Society, UK under Contracts Nos. DH140054, DH160214; The Swedish Research Council; U. S. Department of Energy under Contracts Nos. DE-FG02-05ER41374, DE-SC-0012069.

- [1] R. Aaij *et al.* (LHCb Collaboration), [Synergy of BESIII and LHCb physics programmes](#), LHCb-PUB-2016-025.
- [2] H. N. Li, C. D. Lü and F. S. Yu, *Phys. Rev. D* **86**, 036012 (2012).
- [3] H. Y. Cheng and C. W. Chiang, *Phys. Rev. D* **100**, 093002 (2019).
- [4] I. I. Bigi, A. Paul and S. Recksiegel, *J. High Energy Phys.* **1106**, 089 (2011).
- [5] G. Isidori, J. F. Kamenik, Z. Ligeti and G. Perez, *Phys. Lett. B* **711**, 46 (2011).
- [6] J. Brod, A. L. Kagan and J. Zupan, *Phys. Rev. D* **86**, 014023 (2012).
- [7] H. Y. Cheng and C. W. Chiang, *Phys. Rev. D* **86**, 014014 (2012).
- [8] H. N. Li, C. D. Lü and F. S. Yu, [arXiv:1903.10638](#).
- [9] M. Saur and F. S. Yu, *Sci. Bull.* **65**, 1428-1431 (2020).
- [10] R. Aaij *et al.* (LHCb Collaboration), *Phys. Rev. Lett.* **122**, 211803 (2019).

- [11] B. Aubert *et al.* (BaBar Collaboration), *Phys. Rev. D* **72**, 071102 (2005).
- [12] M. Ablikim *et al.* (BESIII Collaboration), *Chin. Phys. C* **37**, 123001 (2013).
- [13] P. A. Zyla *et al.* (Particle Data Group), *Prog. Theor. Exp. Phys.* **2020**, 083C01 (2020).
- [14] M. Ablikim *et al.* (BESIII Collaboration), *Nucl. Instrum. Meth. A* **614**, 345 (2010).
- [15] C. H. Yu *et al.*, Proceedings of IPAC2016, Busan, Korea, 2016.
- [16] S. Agostinelli *et al.* (GEANT4 Collaboration), *Nucl. Instrum. Meth. A* **506**, 250 (2003).
- [17] S. Jadach, B. F. L. Ward and Z. Was, *Comp. Phys. Commu.* **130**, 260 (2000); *Phys. Rev. D* **63**, 113009 (2001).
- [18] D. J. Lange, *Nucl. Instrum. Meth. A* **462**, 152 (2001); R. G. Ping, *Chin. Phys. C* **32**, 599 (2008).
- [19] J. C. Chen, G. S. Huang, X. R. Qi, D. H. Zhang and Y. S. Zhu, *Phys. Rev. D* **62**, 034003 (2000).
- [20] R.-L. Yang, R. G Ping and H. Chen, *Chin. Phys. Lett.* **31** 061301 (2014).
- [21] E. Richter-Was, *Phys. Lett. B* **303**, 163 (1993).
- [22] H. B. Li and X. R. Lyu, *Natl. Sci. Rev.* **8**, nwab181 (2021).
- [23] M. Ablikim *et al.* (BESIII Collaboration), *Phys. Rev. D* **101**, 052009 (2020).
- [24] M. Ablikim *et al.* (BESIII Collaboration), *Phys. Rev. Lett.* **124**, 241803 (2020).
- [25] M. Ablikim *et al.* (BESIII Collaboration), *Phys. Lett. B* **734**, 227 (2014).
- [26] H. Albrecht *et al.* (ARGUS Collaboration), *Phys. Lett. B* **241**, 278 (1990).
- [27] S. Dobbs *et al.* (CLEO Collaboration), *Phys. Rev. D* **76**, 112001 (2007).
- [28] See the Supplemental Material (to be added by editors) for an illustration of M_{BC}^{tag} versus M_{BC}^{sig} distribution, the comparisons of some typical distributions of the DT candidates between data and MC simulation, the statistical significances for various decay modes, correction factors due to quantum correlation effects, and the systematic uncertainties of various sources in the BF measurements.
- [29] M. Ablikim *et al.* (BESIII Collaboration), [arXiv:2205.14031](https://arxiv.org/abs/2205.14031).
- [30] M. Ablikim *et al.* (BESIII Collaboration), *Eur. Phys. J. C* **76**, 369 (2016).
- [31] M. Ablikim *et al.* (BESIII Collaboration), *Chin. Phys. C* **40**, 113001 (2016).
- [32] M. Ablikim *et al.* (BESIII Collaboration), *Phys. Rev. Lett.* **121**, 171803 (2018).
- [33] G. Wilkinson, *Sci. Bull.* **66**, 2251-2253 (2021).
- [34] S. Malde, C. Thomas, G. Wilkinson, P. Naik, C. Prouve, J. Rademacker, J. Libby, M. Nayak, T. Gershon and R. A. Briere, *Phys. Lett. B* **747**, 9 (2015).
- [35] M. Ablikim *et al.* (BESIII Collaboration), *Phys. Rev. D* **100**, 072006 (2019).
- [36] T. Gershon, J. Libby and G. Wilkinson, *Phys. Lett. B* **750**, 338 (2015).
- [37] T. Evans *et al.*, *Phys. Lett. B* **757**, 520 (2016); **765**, 402(E) (2017).
- [38] Heavy Flavor Averaging Group (HFLAV), (<http://www.slac.stanford.edu/xorg/hflav/charm/>).
- [39] M. Ablikim *et al.* (BESIII Collaboration), *Chin. Phys. C* **44**, 040001 (2020).
- [40] E. Kou *et al.* (Belle II Collaboration), *PTEP* **2019**, 123C01 (2019); **2020**, 029201(E) (2020).
- [41] H. Y. Cheng and C. W. Chiang, *Phys. Rev. D* **81**, 074021 (2010).
- [42] Q. Qin, H. N. Li, C. D. Lü and F. S. Yu, *Phys. Rev. D* **89**, 054006 (2014).

SUPPLEMENTAL MATERIAL

Figure 2 shows the M_{BC}^{tag} versus M_{BC}^{sig} distribution of the accepted DT candidates in data. Detailed selection criteria can be found in context of the main paper.

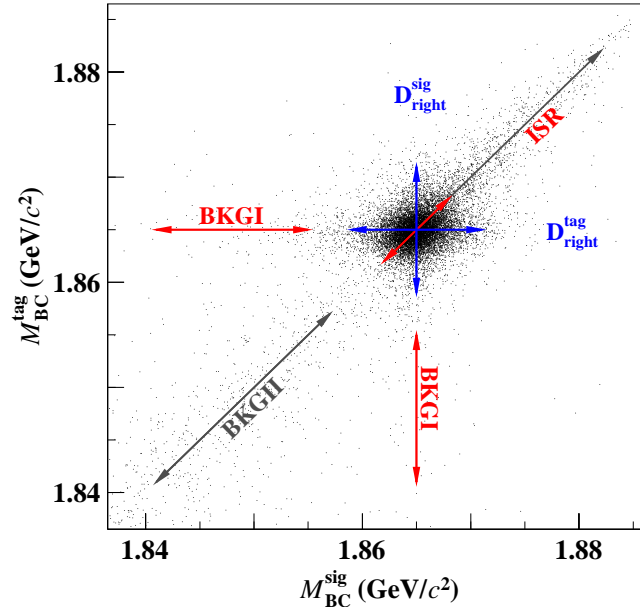


Fig. 2. The M_{BC}^{tag} versus M_{BC}^{sig} distribution of the accepted DT candidates of $D^0 \rightarrow \pi^+ \pi^- \pi^0$ in data. Here, ISR denotes initial state radiation, which spreads along the diagonal direction and extends to the higher M_{BC} sides. The $D_{\text{right}}^{\text{sig}}$ and $D_{\text{right}}^{\text{tag}}$ denotes the signal spreading around $M_{BC}^{\text{sig}} = M_D$ and $M_{BC}^{\text{tag}} = M_D$.

Figures 3 to 11 show comparisons between data and MC simulations for the distributions of invariant mass spectra for the signal DT candidates with more than 100 signal events. The candidates must satisfy additional requirements of $|M_{BC}^{\text{tag(sig)}} - M_D| < 0.006 \text{ GeV}/c^2$ and multiple possible combinations of daughter particles are all plotted when relevant (e.g., all four $\pi^+ \pi^-$ combinations for $D^0 \rightarrow 2\pi^+ 2\pi^- \pi^0$, etc.)

Table 3 summarizes the ST yields of $CP \pm$ tags from the fits to the M_{BC}^{tag} distributions of the accepted ST candidates, the DT yields tagged by $CP \pm$ tags from the 2D fits to the M_{BC}^{tag} versus M_{BC}^{sig} distributions of the accepted DT candidates, and the quantum correlation (QC) factors obtained with the same method as described in Ref. [1] and the necessary parameters quoted from Refs. [2–4].

Table 4 summarizes the statistical significances of the decay modes.

Table 5 summarizes the systematic uncertainties for various sources in the measurements of BFs, which are assigned relative to the measured BFs. They are from the ST yield (N_{tag}), π^\pm tracking efficiency, π^\pm PID efficiency, π^0 and η reconstruction efficiency, daughter BFs, ΔE requirement, K_S^0 rejection, MC statistics, MC generator, 2D fit, and strong phase. For each signal decay, the total uncertainty is obtained by quadratically adding all uncertainties.

-
- [1] M. Ablikim *et al.* (BESIII Collaboration), *Phys. Rev. D* **100**, 072006 (2019).
[2] T. Gershon, J. Libby and G. Wilkinson, *Phys. Lett. B* **750**, 338 (2015).
[3] T. Evans *et al.*, *Phys. Lett. B* **757**, 520 (2016); Erratum: *Phys. Lett. B* **765**, 402 (2017).
[4] Heavy Flavor Averaging Group (HFLAV), (<https://hflav.web.cern.ch/content/charm-physics>).
[5] S. Maldea, C. Thomasa, G. Wilkinson, P. Naik, C. Prouve, J. Rademacker, J. Libby, M. Nayak, T. Gershone and R. A. Briere, *Phys. Lett. B* **747**, 9 (2015).

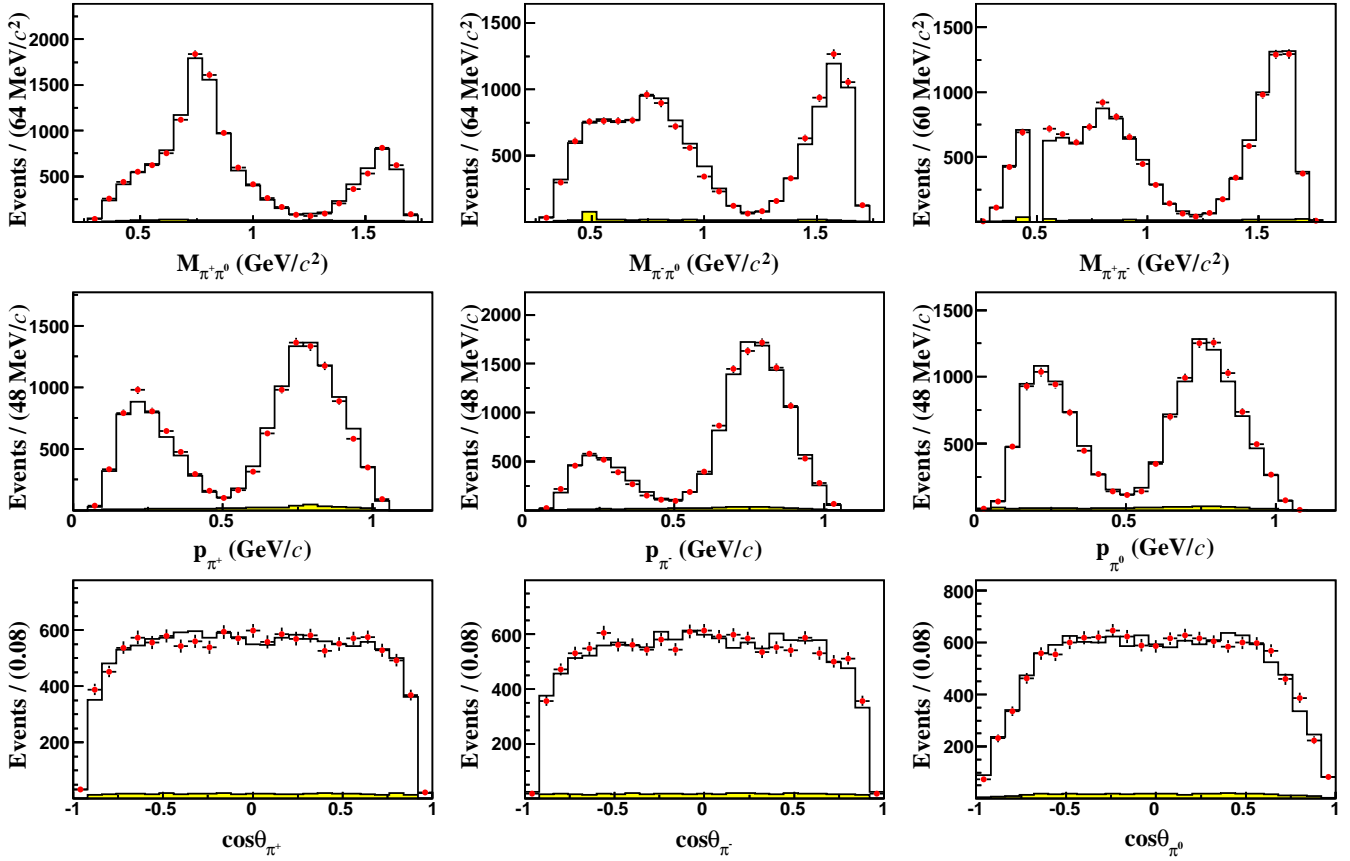


Fig. 3. Comparisons of the distributions of invariant masses of two-body particle combinations, momenta and $\cos \theta$ of daughter particles for the $D^0 \rightarrow \pi^+ \pi^- \pi^0$ candidates between data (points with error bars) and the BODY3 signal MC events (black solid line histograms) plus the MC-simulated backgrounds from the inclusive MC sample (yellow filled histograms).

Table 3. Summary of the ST yields of $CP\mp$ tags (S_{measured}^\pm), the DT yields tagged by $CP\mp$ tags (M_{measured}^\pm), the $CP+$ fraction (f_{CP+}), and the QC factor (f_{QC}). The uncertainties are statistical only. A “/” denotes unmeasured quantities, occurring for one mode with a high-precision external result and for the two CP -eigenstates.

CP mode	$\bar{D}^0 \rightarrow K^+ K^- (CP+)$	$\bar{D}^0 \rightarrow K_S^0 \pi^0 (CP-)$			
	S_{measured}^-	S_{measured}^+			
	57779 ± 287	70512 ± 311			
Decay mode	M_{measured}^-	M_{measured}^+	f_{CP+}	$f_{QC} (\%)$	Uncertainty (%)
$D^0 \rightarrow \pi^+ \pi^- \pi^0$	/	/	0.973 ± 0.017 [5]	93.5 ± 0.5	0.5
$D^0 \rightarrow \pi^+ \pi^- 2\pi^0$	65.7 ± 11.1	169.8 ± 13.9	0.682 ± 0.077	97.4 ± 0.7	0.7
$D^0 \rightarrow 4\pi^0$	/	/	1	93.1 ± 0.5	0.5
$D^0 \rightarrow 3\pi^0 \eta$	/	/	1	93.1 ± 0.5	0.5
$D^0 \rightarrow 2\pi^+ 2\pi^- \pi^0$	37.8 ± 8.3	35.5 ± 6.6	0.438 ± 0.104	100.9 ± 0.9	0.9
$D^0 \rightarrow \pi^+ \pi^- 3\pi^0$	$5.2^{+3.5}_{-2.8}$	$6.8^{+3.4}_{-2.7}$	$0.520^{+0.338}_{-0.269}$	$99.7^{+3.0}_{-2.4}$	3.0
$D^0 \rightarrow 2\pi^+ 2\pi^- 2\pi^0$	$3.5^{+2.8}_{-2.1}$	15.9 ± 3.7	$0.790^{+0.269}_{-0.255}$	$95.9^{+2.2}_{-2.1}$	2.2

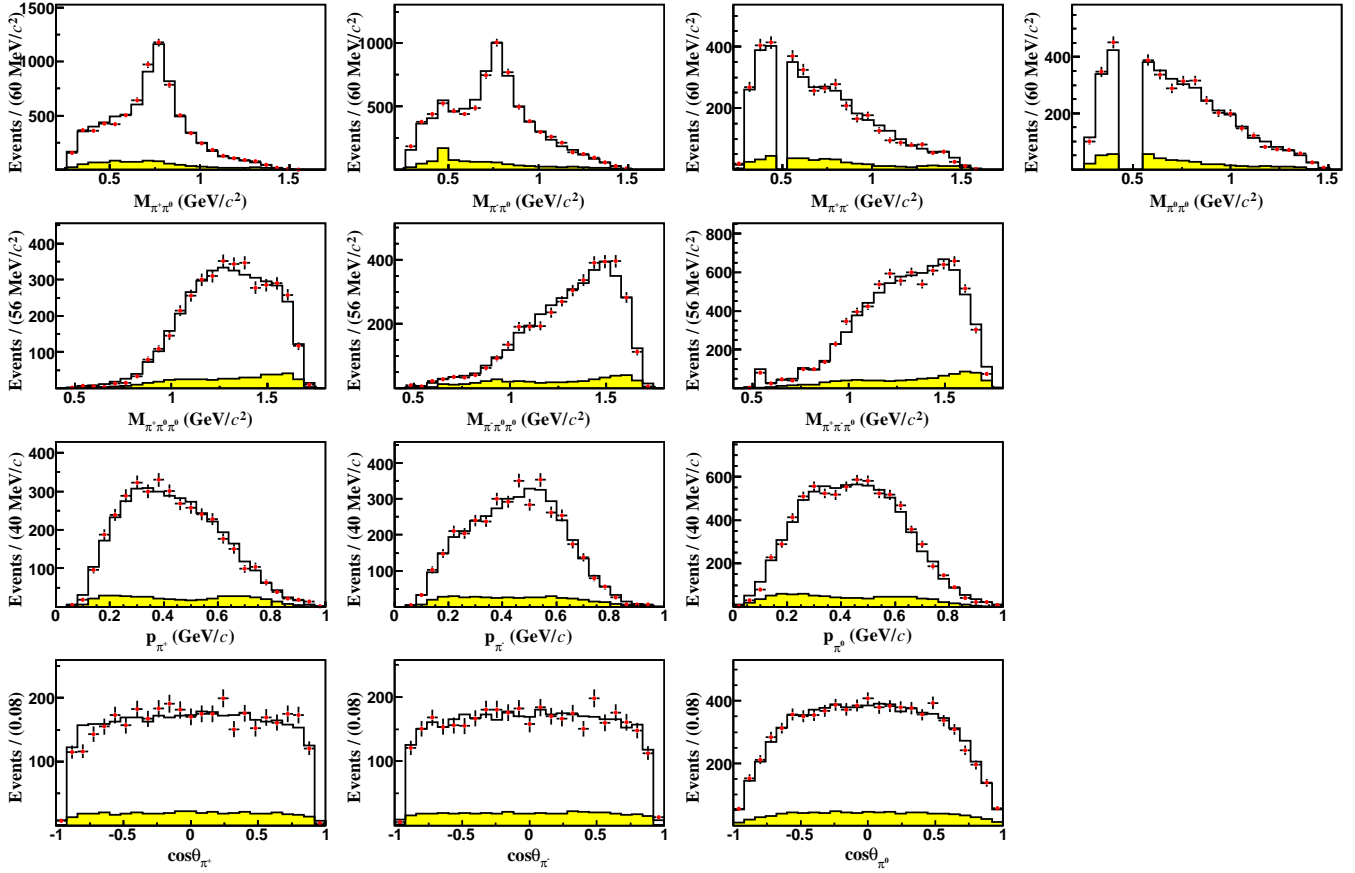


Fig. 4. Comparisons of the distributions of invariant masses of two- or three-body particle combinations, momenta and $\cos \theta$ of daughter particles for the $D^0 \rightarrow \pi^+ \pi^- 2\pi^0$ candidates between data (points with error bars) and the mixing signal MC events (black solid line histograms) plus the MC-simulated backgrounds from the inclusive MC sample (yellow filled histograms).

Table 4. Statistical significances (σ) for various decay modes.

Decay mode	$\pi^+ \pi^- \pi^0$	$\pi^+ \pi^- 2\pi^0$	$\pi^+ \pi^- 2\eta$	$4\pi^0$	$3\pi^0 \eta$	$2\pi^+ 2\pi^- \pi^0$	$2\pi^+ 2\pi^- \eta$	$\pi^+ \pi^- 3\pi^0$	$2\pi^+ 2\pi^- 2\pi^0$	$2\pi^+ \pi^-$
Significance	> 10	> 10	8.7	> 10	> 10	> 10	9.1	> 10	> 10	> 10
Decay mode	$\pi^+ 2\pi^0$	$2\pi^+ \pi^- \pi^0$	$\pi^+ 3\pi^0$	$3\pi^+ 2\pi^-$	$2\pi^+ \pi^- 2\pi^0$	$2\pi^+ \pi^- \pi^0 \eta$	$\pi^+ 4\pi^0$	$\pi^+ 3\pi^0 \eta$	$3\pi^+ 2\pi^- \pi^0$	$2\pi^+ \pi^- 3\pi^0$
Significance	> 10	> 10	> 10	> 10	> 10	> 10	6.8	9.9	> 10	> 10

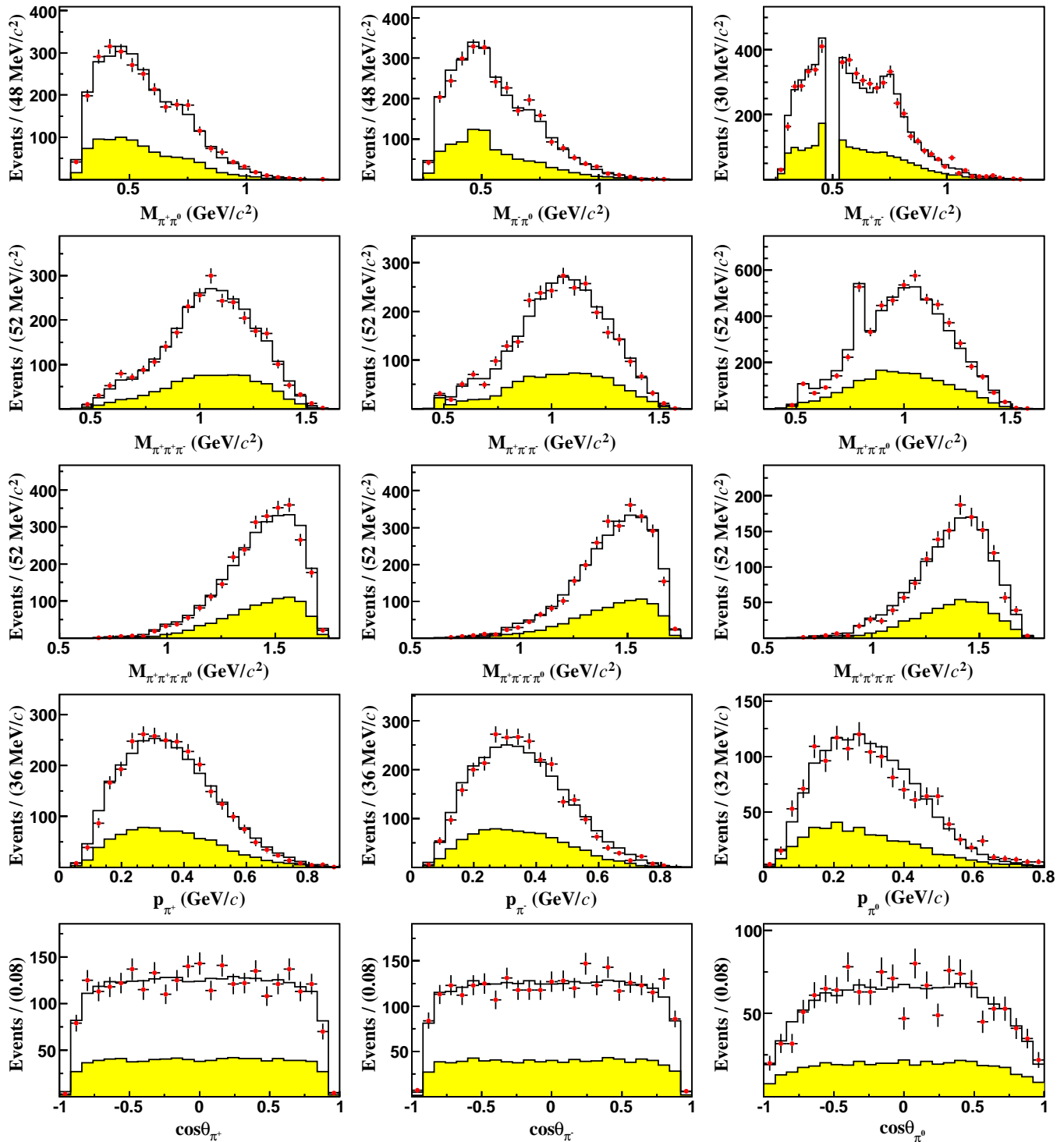


Fig. 5. Comparisons of the distributions of invariant masses of two-, three-, or four-body particle combinations, momenta and $\cos\theta$ of daughter particles for the $D^0 \rightarrow 2\pi^+2\pi^-\pi^0$ candidates between data (points with error bars) and the mixing signal MC events (black solid line histograms) plus the MC-simulated backgrounds from the inclusive MC sample (yellow filled histograms).

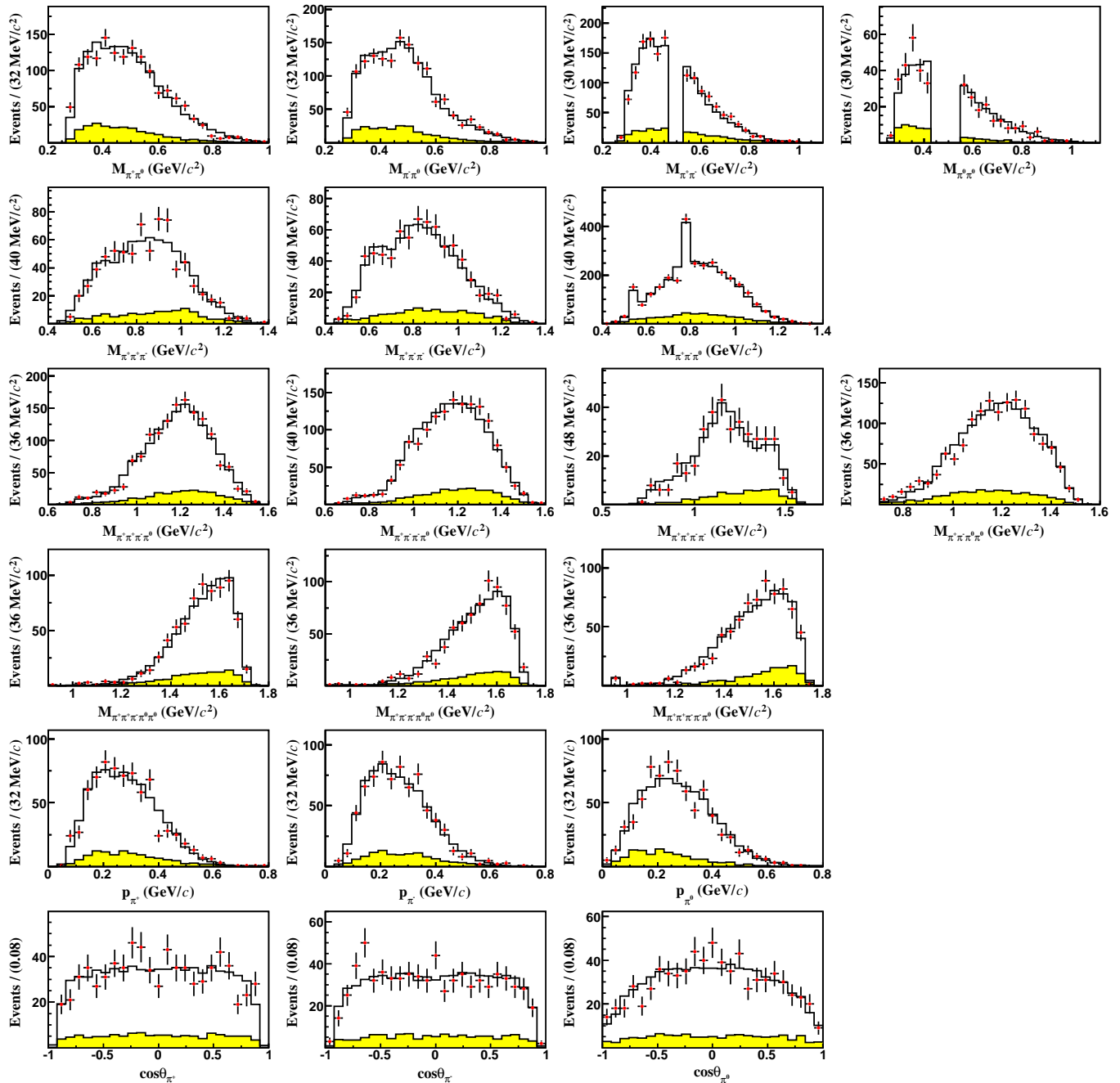


Fig. 6. Comparisons of the distributions of invariant masses of two-, three-, four- or five-body particle combinations, momenta and $\cos\theta$ of daughter particles for the $D^0 \rightarrow 2\pi^+2\pi^-2\pi^0$ candidates between data (points with error bars) and the mixing signal MC events (black solid line histograms) plus the MC-simulated backgrounds from the inclusive MC sample (yellow filled histograms).

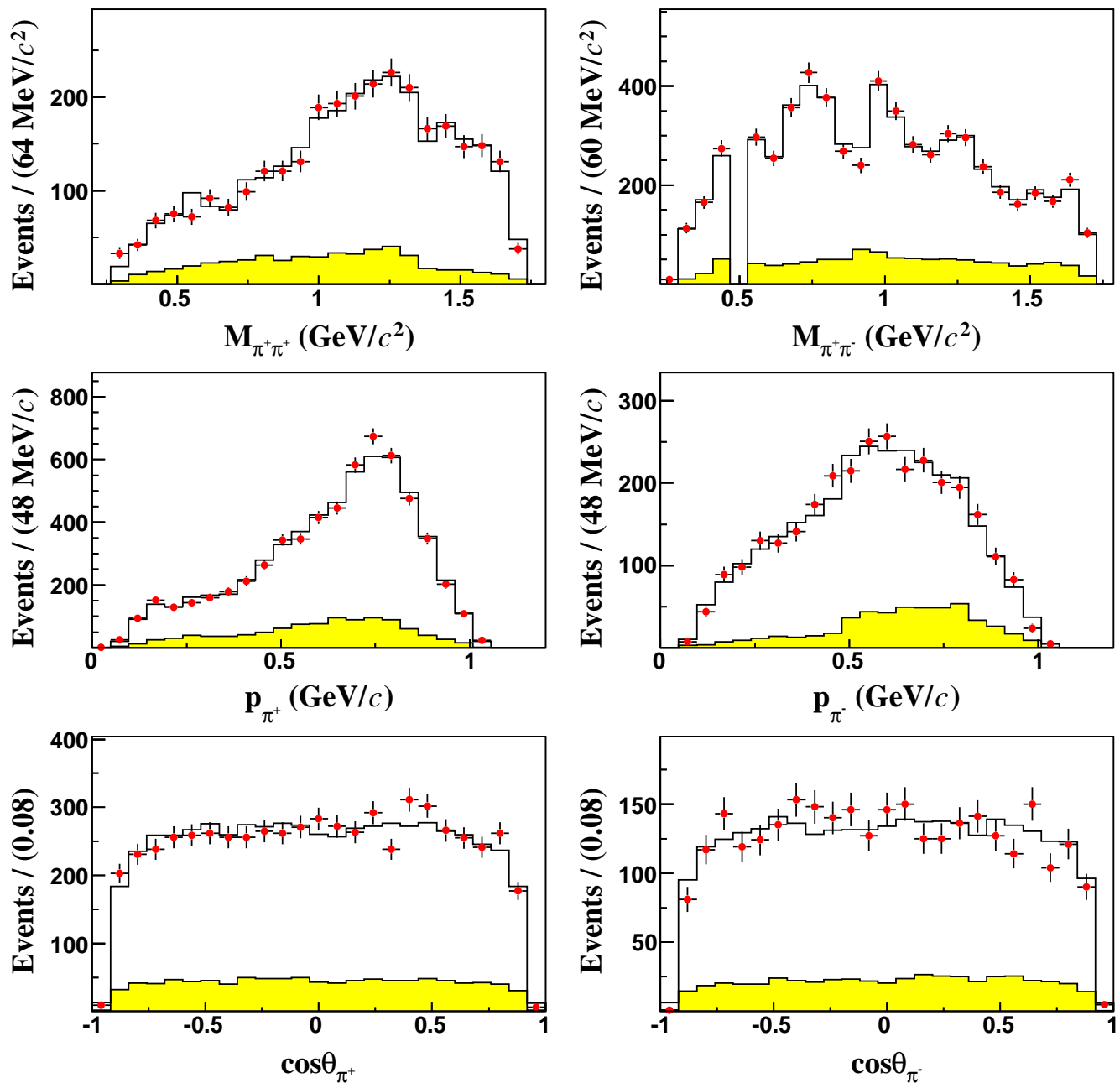


Fig. 7. Comparisons of the distributions of invariant masses of two-body particle combinations, momenta and $\cos\theta$ of daughter particles for the $D^+ \rightarrow 2\pi^+\pi^-$ candidates between data (points with error bars) and the BODY3 signal MC events (black solid line histograms) plus the MC-simulated backgrounds from the inclusive MC sample (yellow filled histograms).

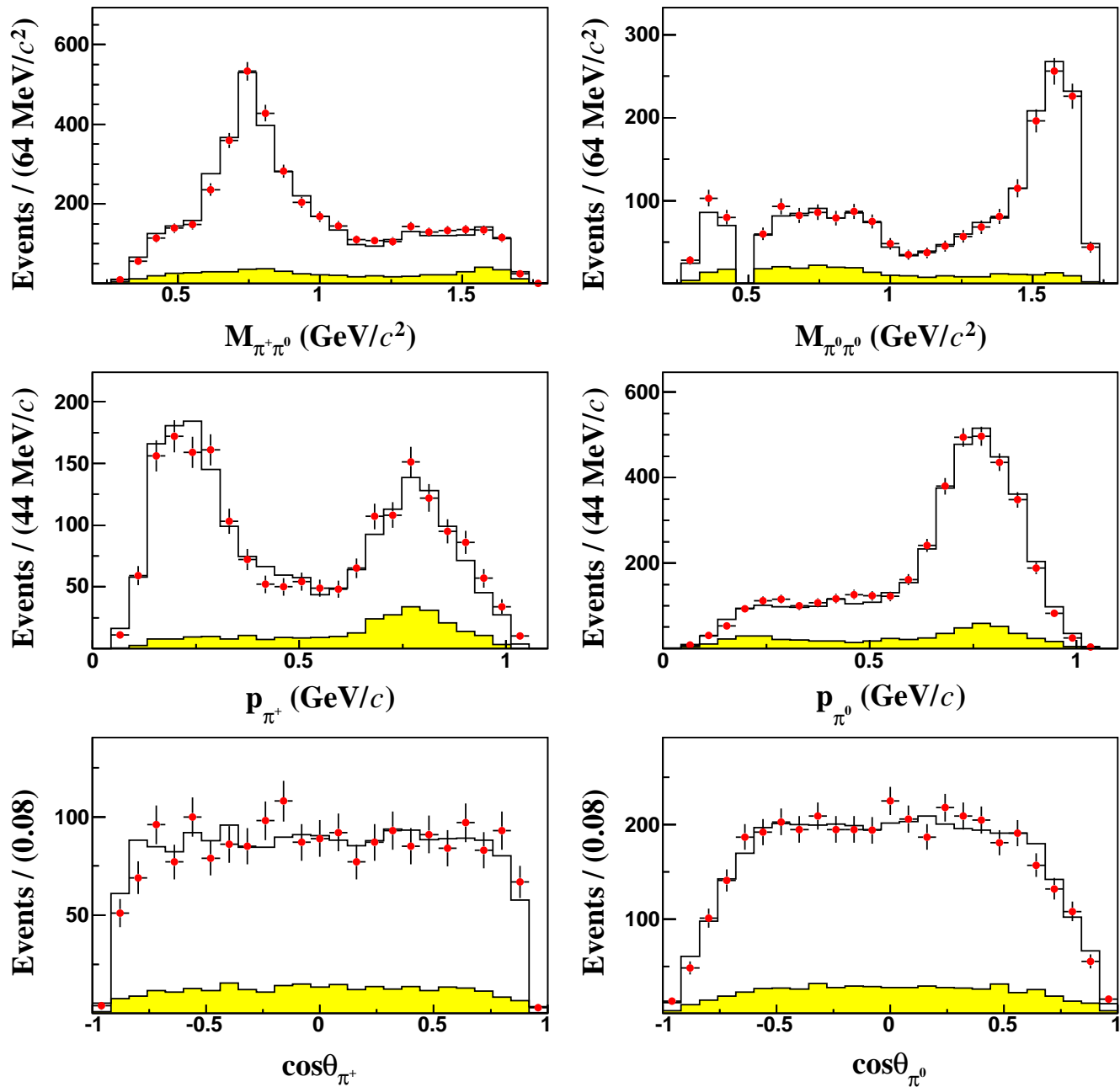


Fig. 8. Comparisons of the distributions of invariant masses of two-body particle combinations, momenta and $\cos\theta$ of daughter particles for the $D^+ \rightarrow \pi^+ 2\pi^0$ candidates between data (points with error bars) and the BODY3 signal MC events (black solid line histograms) plus the MC-simulated backgrounds from the inclusive MC sample (yellow filled histograms).

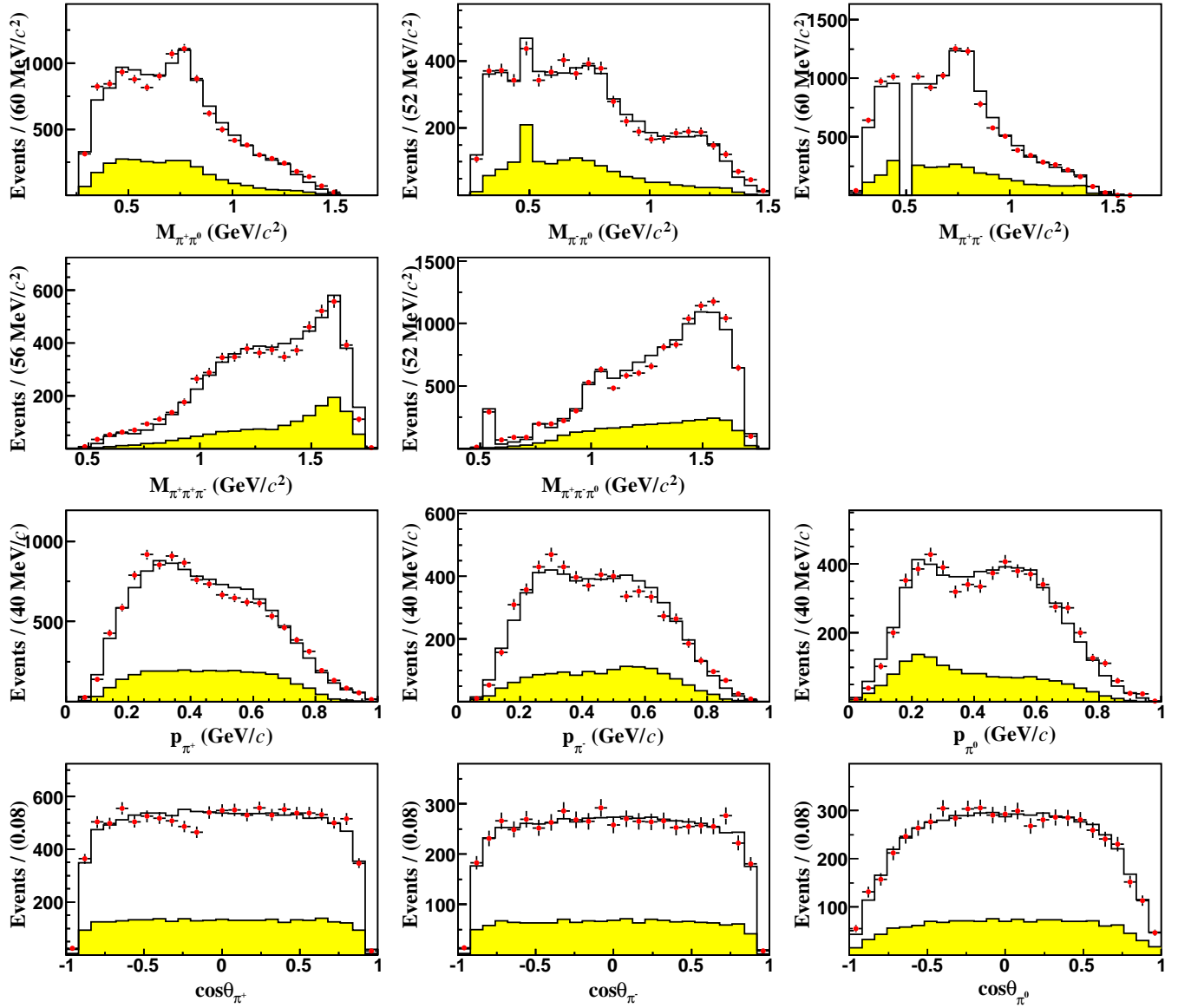


Fig. 9. Comparisons of the distributions of invariant masses of two- or three-body particle combinations, momenta and $\cos\theta$ of daughter particles for the $D^+ \rightarrow 2\pi^+\pi^-\pi^0$ candidates between data (points with error bars) and the mixing signal MC events (black solid line histograms) plus the MC-simulated backgrounds from the inclusive MC sample (yellow filled histograms).

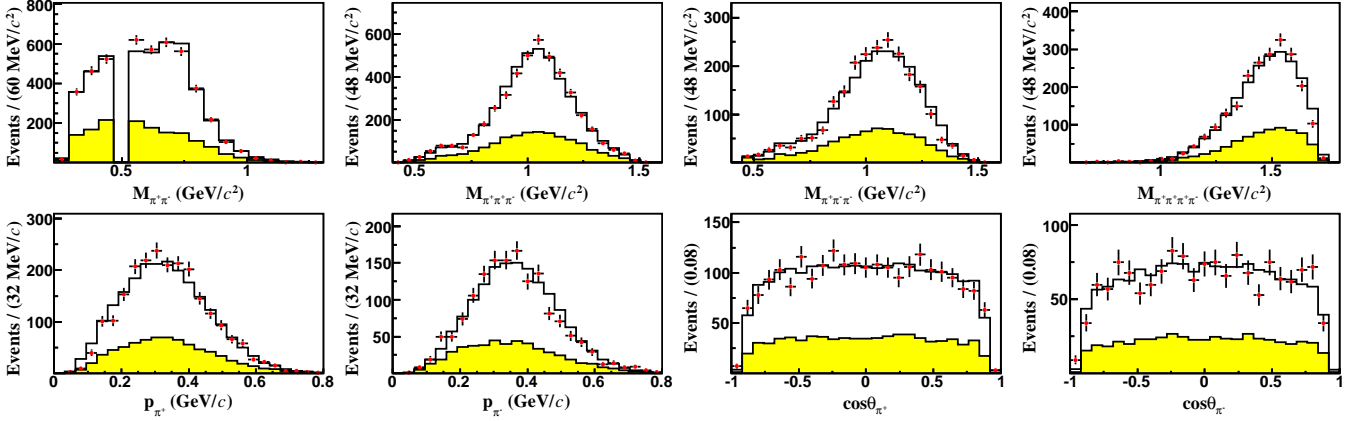


Fig. 10. Comparisons of the distributions of invariant masses of two-, three- or four-body particle combinations, momenta and $\cos\theta$ of daughter particles for the $D^+ \rightarrow 3\pi^+2\pi^-$ candidates between data (points with error bars) and the mixing signal MC events (black solid line histograms) plus the MC-simulated backgrounds from the inclusive MC sample (yellow filled histograms).

Table 5. Systematic uncertainties (%) in the measurements of the BFs for various decay modes.

Source	$D^0 \rightarrow$									$D^+ \rightarrow$
	$\pi^+\pi^-\pi^0$	$\pi^+\pi^-2\pi^0$	$\pi^+\pi^-2\eta$	$4\pi^0$	$3\pi^0\eta$	$2\pi^+2\pi^-\pi^0$	$2\pi^+2\pi^-\eta$	$\pi^+\pi^-3\pi^0$	$2\pi^+2\pi^-2\pi^0$	$2\pi^+\pi^-$
N_{tag}	0.5	0.5	0.5	0.5	0.5	0.5	0.5	0.5	0.5	0.5
π^\pm tracking	0.4	0.4	0.7	–	–	0.8	1.0	0.4	0.8	0.6
π^\pm PID	0.4	0.4	0.4	–	–	0.8	0.8	0.4	0.8	0.6
π^0/η reconstruction	0.4	1.3	1.6	2.3	2.5	0.6	0.7	1.9	1.3	–
2D fit	0.3	0.6	4.4	3.4	4.7	1.7	4.0	3.5	2.3	0.3
ΔE^{sig} cut	0.1	0.1	1.3	0.1	0.1	0.2	0.8	0.1	0.1	0.3
MC generator	0.6	1.5	0.2	3.4	2.8	1.1	1.5	5.3	1.4	0.8
K_S^0 rejection	0.1	0.4	–	7.4	3.5	3.2	8.1	4.7	1.6	0.5
Strong phase	0.5	0.7	–	0.5	0.5	0.9	–	3.0	2.2	–
MC statistics	0.2	0.4	0.5	0.8	0.7	0.5	0.6	0.8	1.0	0.2
Daughter \mathcal{B}	0.03	0.07	1.02	0.14	0.52	0.03	0.51	0.10	0.07	–
Total	1.2	2.4	5.1	9.2	7.0	4.2	9.4	8.7	4.3	1.4
Source	$D^+ \rightarrow$									
	$\pi^+2\pi^0$	$2\pi^+\pi^-\pi^0$	$\pi^+3\pi^0$	$3\pi^+2\pi^-$	$2\pi^+\pi^-2\pi^0$	$2\pi^+\pi^-\pi^0\eta$	$\pi^+4\pi^0$	$\pi^+3\pi^0\eta$	$3\pi^+2\pi^-\pi^0$	$2\pi^+\pi^-3\pi^0$
N_{tag}	0.5	0.5	0.5	0.5	0.5	0.5	0.5	0.5	0.5	0.5
π^\pm tracking	0.2	0.6	0.2	1.1	0.6	0.8	0.2	0.2	1.2	0.6
π^\pm PID	0.2	0.6	0.2	1.0	0.6	0.6	0.2	0.2	1.0	0.6
π^0/η reconstruction	1.0	0.6	1.8	–	1.4	1.4	2.7	3.4	0.8	2.5
2D fit	0.3	0.6	1.7	2.1	1.8	2.3	3.1	3.4	2.8	2.7
ΔE^{sig} cut	0.1	0.1	0.1	0.2	0.1	0.5	0.1	0.1	0.4	0.1
MC generator	1.5	0.8	1.5	3.0	0.7	0.3	4.2	5.7	0.5	1.7
K_S^0 rejection	–	0.8	1.1	3.4	0.8	–	10.2	–	5.6	2.2
Strong phase	–	–	–	–	–	–	–	–	–	–
MC statistics	0.3	0.3	0.6	0.4	0.6	0.6	1.3	0.8	0.8	0.9
Daughter \mathcal{B}	0.07	0.03	0.10	–	0.07	0.51	0.14	0.52	0.03	0.10
Total	1.9	1.8	3.2	5.3	2.8	3.1	11.9	7.5	6.6	4.8

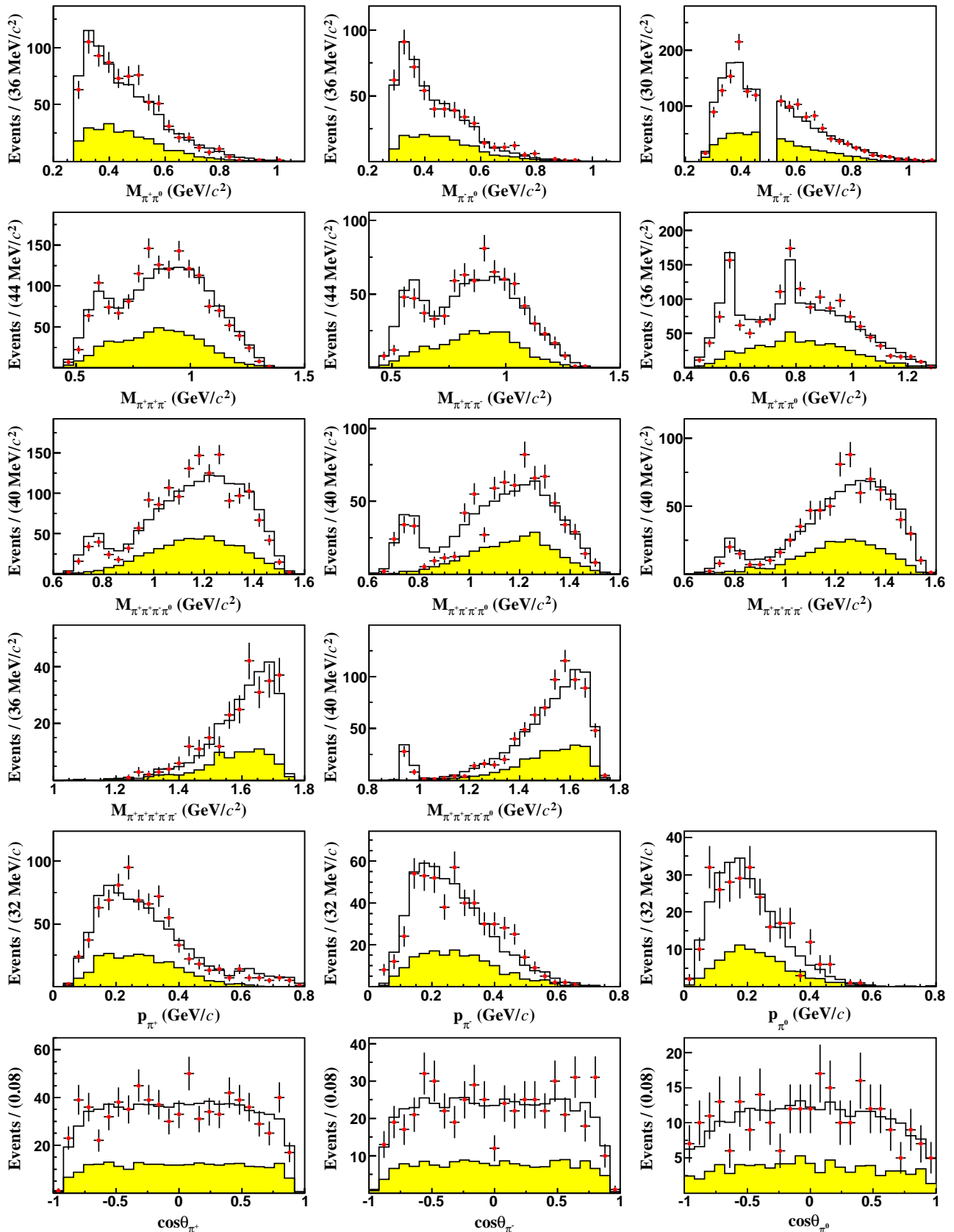


Fig. 11. Comparisons of the distributions of invariant masses of two-, three-, four- or five-body particle combinations, momenta and $\cos\theta$ of daughter particles for the $D^+ \rightarrow 3\pi^+2\pi^-\pi^0$ candidates between data (points with error bars) and the mixing signal MC events (black solid line histograms) plus the MC-simulated backgrounds from the inclusive MC sample (yellow filled histograms).